The Interaction Between Climate Forcing and Feedbacks

A. Gettelman[1*], T. Eidhammer[2], M. L. Duffy[2], D. T. McCoy[3], C. Song[3], D. Watson-Parris[4]

[1]Pacific Northwest National Laboratory, Richland, WA, USA
[2]NSF National Center for Atmospheric Research, Boulder, CO, USA
[3]Department of Atmospheric Sciences, University of Wyoming, Laramie, WY, USA
[4]University of California San Diego, La Jolla, CA, USA

Key Points:

- Parametric uncertainty of Aerosol Forcing and Cloud Feedbacks are large
- Aerosol Forcing and Cloud Feedbacks are related through cloud processes and depend on the mean state of clouds
- Warm rain formation and ice processes are critical sensitivities that couple forcing and feedback

[*]Formerly at NCAR

Corresponding author: Andrew Gettelman, andrew.gettelman@pnnl.gov

Abstract

A Perturbed Parameter Ensemble (PPE) with the Community Atmosphere Model version 6 (CAM6) is used to better understand the sensitivity of simulated clouds to both aerosol forcing and cloud feedbacks and the interactions between them. Aerosol forcing through aerosol-cloud interactions is mostly negative (a cooling) due to shortwave radiation, while feedbacks are positive or negative in different regions due to contrasting longwave and shortwave effects. Both forcing and feedbacks are related to the mean climate state. Higher magnitude cloud radiative effects generally mean larger net forcing and larger net feedback. Aerosol forcing is broadly related to the susceptibility of clouds to drop number. Feedbacks are less related to susceptibility, and in different regions. Aerosol forcing and cloud feedbacks are anti-correlated in the CAM6 PPE such that stronger negative forcing is associated with stronger positive feedbacks. Even the processes governing forcing and feedback sensitivity in the PPE are similar. These include the warm rain formation process, ice loss processes and deep convective intensity.

Plain Language Summary

A climate model is run many times with modified parameters to see how the parameters affect key aspects of climate change. The paper focuses on two aspects of climate change. First, the cloud response to aerosol particles tends to create a cooling, which partially offsets greenhouse gas warming, but the magnitude of the cooling is not well known. It varies a lot in the model when parameters are changed. Second, the paper examines the cloud response to surface temperature increases, called cloud feedbacks, which are the largest uncertainty in estimating the level of future climate change. Cloud feedbacks are also sensitive to parameters. The results show that the cloud feedbacks and aerosol forcing changes are similar but opposite in the model: the cooling and warming generally increase together. This occurs because they are linked to similar parameters, which indicate sensitivity to critical processes, including how rain forms, and how much ice is in the atmosphere.

1 Introduction

Uncertainties in predicting the evolution of the Earth's climate arise from complexity in the response of the system to anthropogenic radiative forcing, and in the actual level of radiative forcing. The largest uncertainty in the fast response of the climate system is due to the response of clouds to changes in the environment: cloud feedbacks (Gettelman & Sherwood, 2016; S. Sherwood et al., 2020). In addition, the largest uncertainty in anthropogenic radiative forcing is the response of clouds to aerosol perturbations ("Summary for Policymakers", 2021), often termed Aerosol-Cloud Interactions (ACI). These perturbations are significant but complex (Bellouin et al., 2020). More aerosol particles increase cloud drop numbers and lead to brighter clouds (Twomey, 1974) and potentially longer-lived or thicker clouds (Albrecht, 1989). To assess these processes globally, comprehensive Earth System Models (ESMs) with atmospheric components that include a detailed representation of cloud physics, aerosol physics as well as the interactions between them must be used. The scale of these models, typically 100km horizontal, several hundred meter vertical and 10-30 minute time-steps is too coarse to explicitly resove key cloud and aerosol processes and therefore introduces very large uncertainties in cloud physics representations.

Much has been written about analyzing model and observational analogs for ACI (Bellouin et al., 2020) and cloud feedbacks (S. Sherwood et al., 2020). Many of the processes which control both ACI and cloud feedback responses are the same. For example, extensive decks of bright liquid cloud at the top of the Planetary Boundary Layer (PBL) over the darker ocean significantly cool the planet by reflecting solar radiation

back to space. These clouds exist due to an inversion that traps moist ocean air near the surface. The strength of that inversion has been shown to be important in cloud formation and maintenance, and how that inversion changes over time is important for how clouds will respond to climate change: how thick they are and their propensity to rain (S. C. Sherwood et al., 2014). Similarly, aerosols impact clouds by changing the drop population (more aerosols implies more cloud drops), and how these clouds evolve may also be determined by the inversion at the top of the boundary layer (Ackerman et al., 2004), and their propensity to rain.

Given the importance of cloud processes at the nexus of forcing and feedback, there has yet been little work on the interaction between these two effects beyond global means. Kiehl (2007) noted that in ESMs there was a relationship across models between the total response to climate change and aerosol forcing. This was updated by Forster et al. (2013) to show less of an overall relationship. The latest generation of ESMs show no relationship (Smith et al., 2020), though Watson-Parris & Smith (2022) find a relationship between forcing and feedback when constrained on historical surface temperature. Gettelman et al. (2016) noted other process level interactions such as an 'Aerosol Mediated Cloud Feedback' whereby the mechanism for cloud feedbacks occurs by climate change altering aerosol populations. An example noted by Gettelman et al. (2016) is that increasing wind speeds over the S. Ocean increase sea spray and cloud drop number, brightening clouds. This negative cloud feedback is mediated by aerosols. This work will seek to examine the relationship between cloud feedbacks and aerosol forcing of clouds in more detail by taking advantage of a unique dataset with a modern ESM.

Here we will look at the interaction between aerosol forcing and cloud feedbacks with a large Perturbed Parameter Ensemble (PPE) from the Community Atmosphere Model version 6 (CAM6). The CAM6-PPE uses parameter perturbations to sample model structural uncertainty, and produce a wide range of climates resulting from very different adjustments to cloud and aerosol processes. Similar PPEs have been used to understand model parametric uncertainty (Qian et al., 2018), constrain aerosol forcing (Regayre et al., 2023; Lee et al., 2016) and low cloud feedbacks (H. Zhang et al., 2018). In this work, we will use the CAM6-PPE to better understand the interaction between forcing and feedback with the goal of understanding critical process and how they interact.

Section 2 describes the data and methods to be used. Section 3 presents detailed results of forcing sensitivity, feedback sensitivity and their interactions. Discussion is in Section 4 and conclusions are in Section 5.

2 Methods

The simulations used for this analysis are from the Community Atmosphere Model version 6 (CAM6) PPE. The CAM6-PPE is described in detail by Eidhammer et al. (2024). It consists of 263 ensemble members in which latin hypercube sampling is used to modify 45 parameters in the microphysics, convection, turbulence and aerosol schemes. Note that one of the simulations did not complete, and that two pairs of parameters are varied together, so effectively 43 parameters are varied. These atmospheric parameters are typically the most uncertain in many climate models and contain many variables which alter cloud and aerosol processes. Parameter ranges are chosen to be physically plausible for each parameter. We also will subset the parameter space based on physically realistic climates as described below. Simulations are run with an atmosphere-land configuration for 3 years, for Present Day (PD) climatological boundary conditions, repeating climatological averaged Sea Surface Temperatures (SSTs) each year. In addition, two other additional sets of 263 simulations are run with the same parameters. In one set, SSTs are uniformly increased by 4K to assess the cloud response to warming, following Cess et al. (1989), termed SST4K. In the other set of 263 simulations, PD SSTs and the

same boundary conditions are used, except aerosol emissions are set to 1850 'Pre-Industrial' levels (hereafter PI simulations).

The principle we will exploit is that different parameters modify different specific processes in the cloud physics (e.g., frequency or intensity of deep convection, rain formation processes, freezing and ice nucleation processes, etc). The changing balance of processes alters the climate. First, we will use the PPE to understand if forcing and feedbacks depend on the base climate state of those simulations. Then we will use the PPE to understand which parameters give rise to variations and sensitivity in forcing and feedbacks. Finally we will explore the relationship between aerosol forcing and cloud feedbacks. The parameters map to the underlying physical mechanisms. While the parameters in the PPE are model specific, the process representations are very similar to (or even the same as) other modern ESMs. Thus the results may have more general application since the relationships we elucidate are well founded in processes, not just in parameters.

As described by Gettelman et al. (2019), the aerosol induced cloud forcing (ACI, or just 'forcing') is defined as the change in Cloud Radiative Effect (CRE) between simulations with Present Day (PD) and Pre-Industrial (PI) aerosol emissions. Typically we are concerned with the Shortwave (SW) cloud forcing (SW ACI = ΔSWCRE), but there is also Longwave (LW) forcing (LW ACI = ΔLWCRE). Cloud feedbacks are defined as the kernel adjusted cloud feedbacks (Soden et al., 2008) using the kernels from Zelinka et al. (2012) as applied by Duffy et al (2023). The kernels adjust LW and SW CRE to remove effects of changes to the atmospheric temperature and water vapor, and the effect of a changing surface albedo.

To constrain the simulations for fidelity against observations we also compare them to observations of radiative fluxes and clouds from the CERES (Clouds and the Earth's Radiant Energy System) satellite Energy Balanced and Filled (EBAF) products (Loeb et al., 2018).

Finally, for analysis of the simulations and sensitivity to parameters (and hence processes), we use Gaussian process emulators (Watson-Parris et al., 2021) trained on the PPE ensemble to determine the sensitivity of forcing and feedbacks to each parameter.

3 Results

First we illustrate the parametric uncertainty (i.e. the PPE spread) of feedbacks and forcing (Section 3.1). Then we examine how aerosol forcing is related to the mean state and to different parameters, which are both indicative of specific processes (Section 3.2). Next we will do the same analysis for cloud feedbacks (Section 3.3) and then we will explore the interaction between aerosol forcing and cloud feedbacks (Section 3.4)

3.1 PPE Mean and Spread

Figure 1 illustrates the global mean change in SW (Figure 1A), LW (Figure 1B) net TOA radiation (Figure 1C) and change in total cloud fraction (Figure 1D) for the 263 PPE members. The forcing in Figure 1A and B is the change in CRE, while the feedbacks are the kernel-adjusted feedbacks. The spread estimates the parametric uncertainty in forcing and feedback.

The spread in net ACI forcing is only $\sim$2Wm^{-2}, because the global mean SW and LW are of opposite sign and are strongly anti-correlated, resulting in a fairly narrow range in total net TOA change (Figure 1C). The anti-correlation is not as strong for cloud feedbacks where the SW and LW components are both positive in most ensemble members. Note that the TOA change for feedbacks includes a significant change NOT associated with clouds, but rather for the clear sky (due to a warmer surface). There is also far less

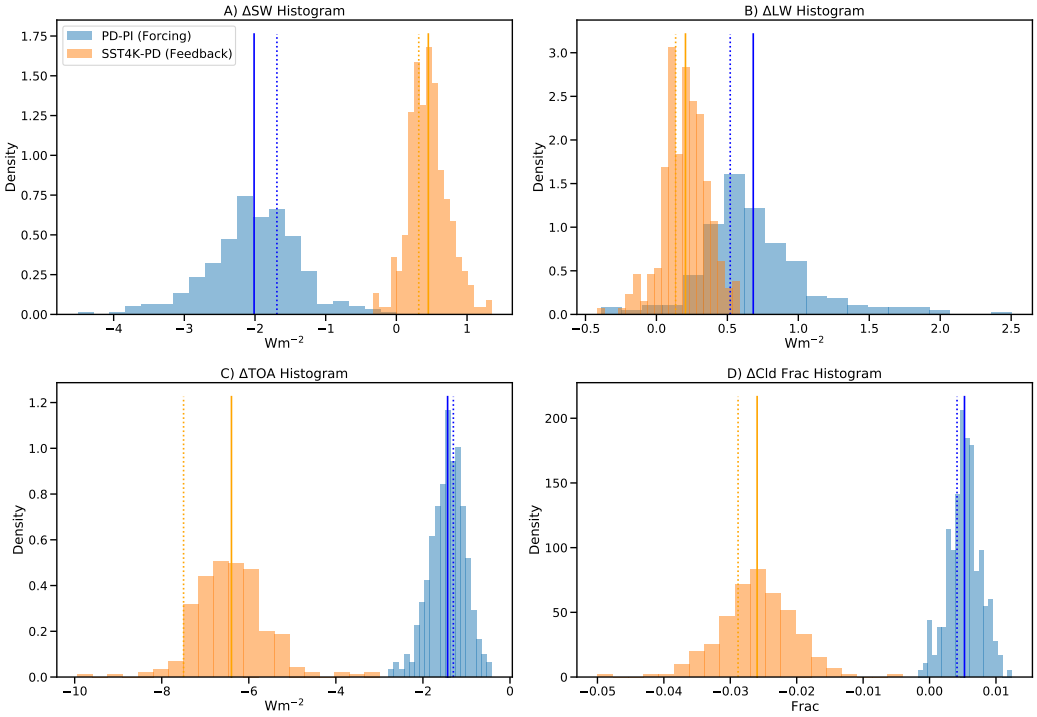

Figure 1. Histograms of global A) TOA SW change, B) TOA LW change, C) Net TOA change and D) Cloud Fraction change for Present Day - Pre-Industrial (Aerosol Forcing, Blue) and SST+4K - Present Day (Feedback response, orange). Forcing is change in TOA Cloud Radiative Effect (CRE) and feedbacks are the kernel adjusted cloud feedbacks as descried in the text. Solid lines are the mean of the distribution, dotted lines are results with the default CAM6 parameter settings.

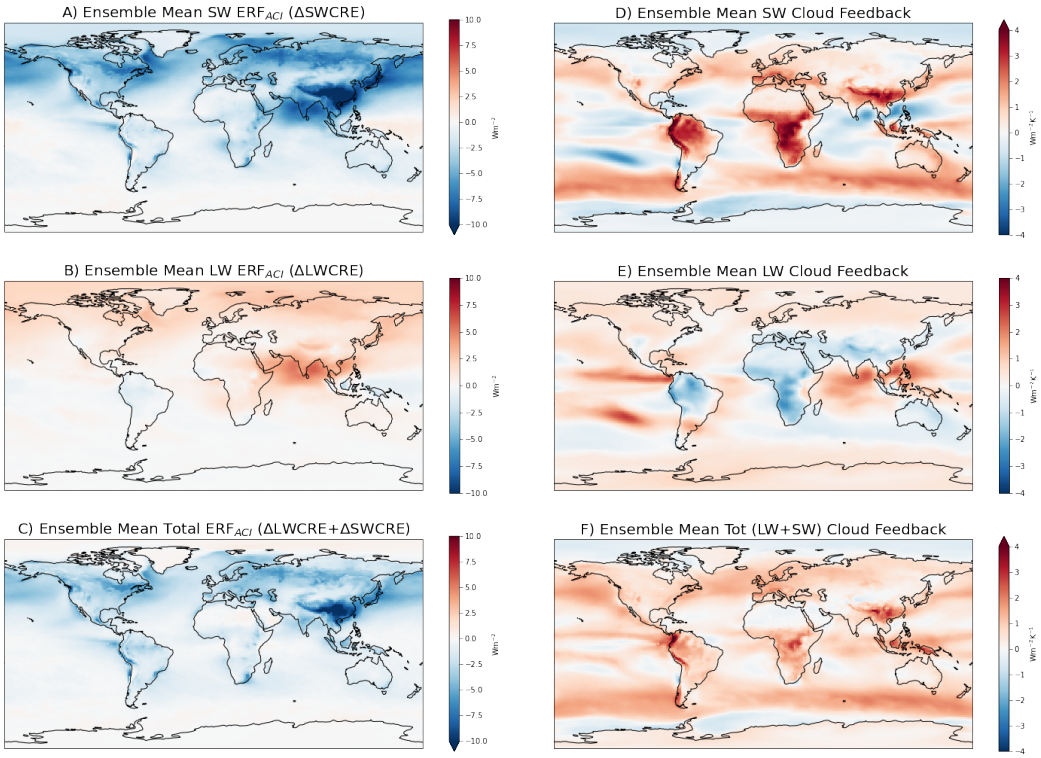

Figure 2. PPE ensemble means of Aerosol Cloud Interactions (Forcing) for the A) SW, B) LW and C) Total (LW+SW) as well as Cloud Feedbacks for the D) SW, E) LW and F) Total (LW+SW).

cloud fraction change (Figure 1D), both the mean and PPE spread, for aerosol forcing than for cloud feedbacks.

Figure 2 illustrates the ensemble mean cloud forcing (ACI) as the change in CRE between present (PD) and pre-industrial (PI) simulations for the SW (Figure 2A), LW (Figure 2B) and Net (Figure 2C). Figure 1A and B indicate that for both forcing and feedback, the ensemble mean (solid vertical lines in Figure 1) is similar to the default (dotted vertical lines in Figure 1). We have verified that this is qualitatively the case for maps as well by mapping the default case individually: the ensemble mean just provides better statistics to smooth out noise in the short 3 year simulations. ACI is strongest in the SW, concentrated in the N. Hemisphere, with the largest values over oceans downwind of source regions (N. Pacific, N. Atlantic and N. Indian Ocean), and a strong SW signal over China. SW is larger than LW, with the largest LW effect near India, due perhaps to aerosol effects on tropical ice clouds, which mostly cancel the SW effects. There is virtually no aerosol forcing in the S. Hemisphere. SW and LW are of opposite sign in most regions, but there is not a 1:1 correlation in the magnitude. Net ACI becomes weakly positive over the Arctic ocean due to lack of SW cooling from clouds over a bright ice-covered surface.

Figure 2 also illustrates the ensemble mean cloud feedbacks for the SW (Figure 2D), LW (Figure 2E) and total (Figure 2F). As with forcing, the ensemble mean is qualitatively similar to the default case. There are significant positive (and net) SW Cloud Feedbacks over tropical continents in convective regions, as well as in the mid-latitude storm

tracks in both hemispheres. In the tropical convecting regions, the two mechanisms controlling cloud feedbacks are the increase in altitude of high clouds and a reduction in anvil cloud area (S. Sherwood et al., 2020). The increase in the altitude of high clouds is a positive LW cloud feedback (the red area over the tropical west Pacific/Indian ocean). The reduction in anvil cloud area should have competing LW positive and SW negative effects as illustrated in Figure 2D and Figure 2E. The net cloud feedbacks are positive, except over polar regions with frequent sea-ice coverage.

3.2 Forcing

We start by focusing on the aerosol forcing, again defining ACI as the change in CRE between PD and PI simulations (either LW, SW or Net=SW+LW). First we attempt to understand whether ACI is related to properties of the mean state climate. Aerosol forcing is a series of processes that might be reflected in correlations between the forcing and the mean state. Increases in emissions increase aerosols (largely sulfate) which increase the Cloud Condensation Nuclei (CCN) and Ice Nuclei (IN), and hence cloud drop and ice crystal number. This might affect cloud fraction and/or cloud mass (Ice Water Path [IWP] and Liquid Water Path [LWP]). The mean state might make the clouds more or less 'susceptible' to these changes. For example: higher base state sulfur and higher CCN and/or drop number for PI conditions might make a perturbation to sulfur less important. Or having more clouds (either larger negative SW CRE or higher cloud fraction) might result in more 'marginal' clouds that could be affected by ACI.

We focus on the mean state climate of the PI simulations. In the present day, some of the correlation between mean state and aerosols is due to anthropogenic aerosol forcing, and we are interested in the 'unaffected' state. We start with correlations of global mean state properties with global mean ACI. Figure 3 illustrates that the magnitude of globally averaged Net ACI is correlated with several properties of the mean state: Total Cloud Fraction (Figure 3A), Sulfate (SO_4) Burden (Figure 3B), CCN at 0.2% supersaturation (Figure 3C) and Cloud Top Drop Number (Nc, Figure 3D). We looked at several PI mean state properties not strongly correlated with global mean forcing: LWP and IWP. Column drop number is similar to cloud top drop number (Figure 3D).

The orange points are the sub-set of simulations whose mean annual value of SW CRE is within ± 5 Wm^{-2} of the observed CERES EBAF annual global mean (-45.3 Wm^{-2}). This constraint is a gross measure of whether the 'climate' in any simulation (specifically the cloud climatology) is similar to present day observations. The slopes (orange lines) are qualitatively similar (with lower correlation) if we consider only the constrained data rather than all the data for most of the variables except cloud coverage. The red dot is the 'default' parameter set for CAM6.

Figure 3A indicates that as total mean state cloud fraction increases, net ACI increases in magnitude (negative). This implies more cloudiness may mean more marginal or thin clouds that are more susceptible to changes. As mean PI sulfate burden increases, net ACI forcing is reduced (lower magnitude) (Figure 3B) with a similar relationship for CCN (Figure 3C). These both indicate that PI environments with higher sulfur and more CCN are less sensitive to additional sulfur, a result noted in other models (Carslaw et al., 2013). There is also a relationship between cloud top drop number and Net ACI forcing (Figure 3D) whereby higher PI drop numbers give rise to larger forcing, which seems to work in the opposite way to more PI CCN. In general, these correlations using global means are quite low. SW ACI only correlations are a little stronger (not shown). The CERES constrained simulations have similar correlations to all simulations, with lower magnitude (except for total cloud coverage, where constrained simulations have a smaller correlation of the opposite sign).

To understand these relationships better, we can map the correlations at each point to determine what regimes are important. Figure 4 illustrates the same relationships as

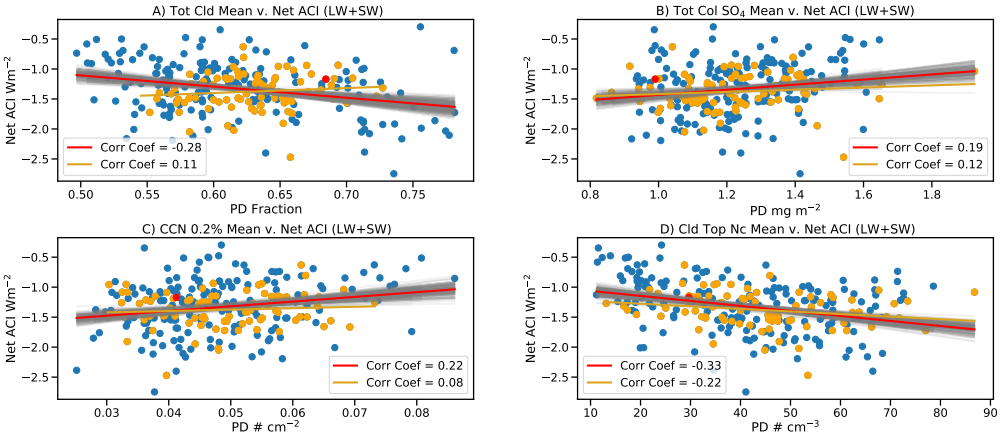

Figure 3. Global correlations between mean state for A) Total Cloud Fraction, B) Total Column Sulfate, C) CCN at 0.2% supersaturation and D) Cloud top drop number with Pre-Industrial aerosols (horizontal axis and the Net ACI forcing (PD-PI, vertical axis). Blue points: all simulations, red line, linear regression. Orange indicates those 87 simulations whose global mean PD Shortwave Cloud Radiative Effect is within ±5 Wm^{-2} of the CERES EBAF global annual mean. Orange line is the linear regression of these points. Default CAM6 parameters shown as the red dot.

Figure 3 using PI mean climate and aerosol net forcing (PD - PI change in SW+LW CRE) but now as a map at each point. An expanded set of mean state indicators are illustrated. The linear correlation coefficient at each point is plotted, with the stippling indicating regions which are NOT significant based on a bootstrap fit. Maps are similar if only the simulations constrained by the observed satellite SW CRE climatology are used, but with less significance (similar to Figure 3). We have examined the LW and SW components separately, and in general net ACI forcing is dominated by the SW as seen in Figure 2.

The weak global correlations in Figure 3 belie stronger regional correlations, which can be of different sign between regions and hence cloud types. In many cases there are opposite sign correlations over the Arctic ocean where the SW ACI goes to zero (Figure 2A) and the positive LW ACI component dominates (Figure 2C). The opposite sign correlation is due to the local ACI being dominated by the LW and changing sign. There is a strong positive correlation between the net ACI forcing (net ACI = ΔSWCRE + ΔLWCRE) and the PI SW Cloud Radiative Effect (SW CRE, Figure 4G) at low latitudes over the ocean. Stronger negative PI mean state SW CRE in the subtropics is associated with stronger negative ACI. Similar patterns of opposite sign (since SW CRE is negative) are seen for total cloud coverage (Figure 4A), LWP (Figure 4B), LW CRE (Figure 4F), cloud top liquid number (Figure 4I) and column drop number (Figure 4J). Column drop number is integrated to the top of the atmosphere. CCN effects (fewer CCN in PI result in stronger magnitude ACI) are mostly positive throughout the N. Hemisphere. (Figure 4E). Stronger positive ACI at high latitudes (dominated by the LW) is associated with more ice fraction at high latitudes (Figure 4H).

Figure 3 indicates that stronger magnitude net ACI is associated with PI climates that have radiatively thicker sub-tropical liquid clouds. These 'radiatively thicker' clouds have larger magnitude cloud radiative effect due to being more extensive, with higher drop number and LWP. Stronger net ACI can also be associated with less PI CCN at middle and high latitudes and less sulfate over the land regions in mid-latitudes. To some extent these effects will offset (higher PI CCN should lead to higher Nc), but the effects

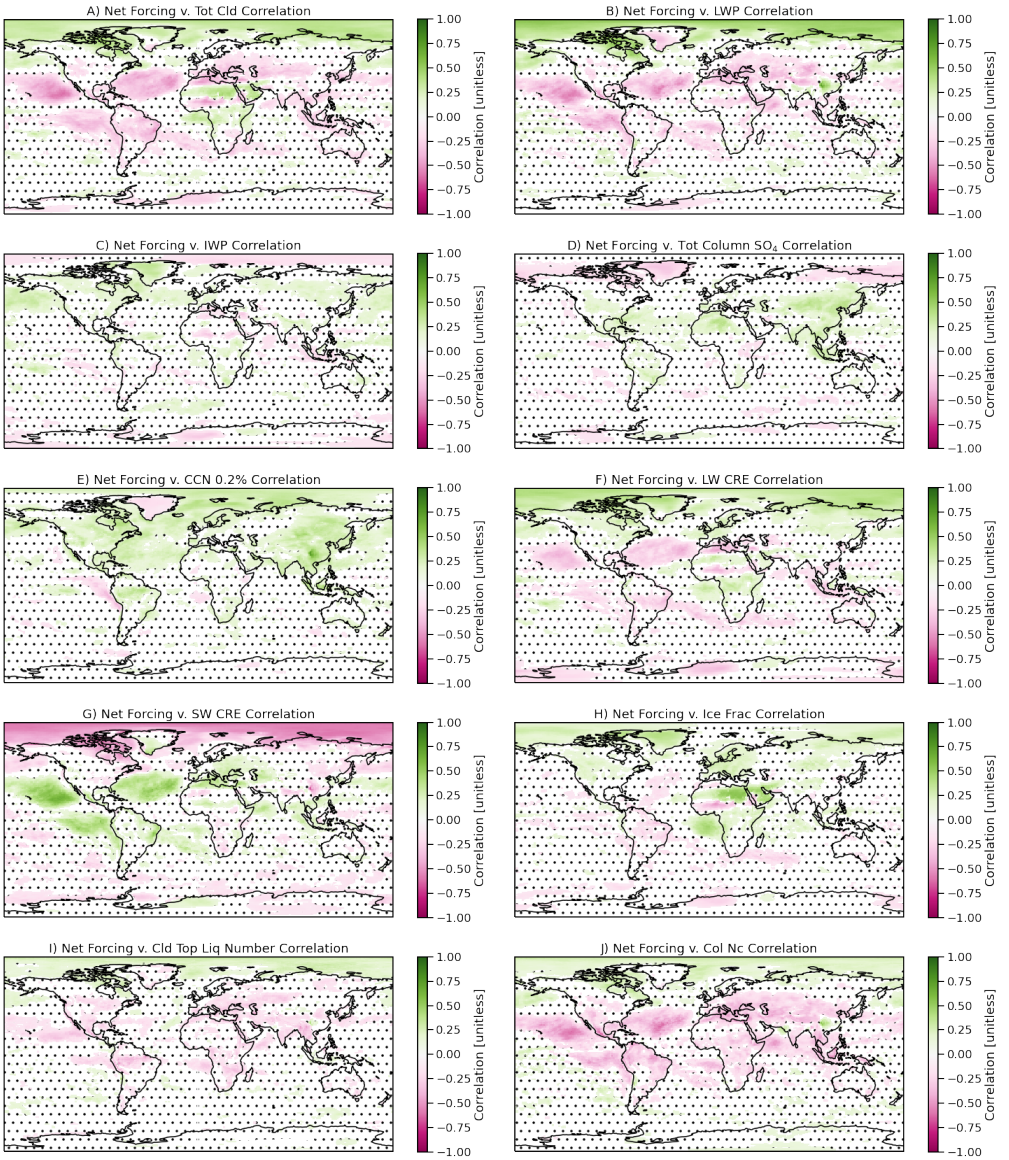

Figure 4. Map of linear correlation coefficient at each point between mean state in PI and the ACI forcing (PD-PI) for different variables. Non-significant points are stippled. Significance is determined by a bootstrap fit.

occur in different regions (subtropical clouds, and more mid-latitude for CCN). The subtropical regions noted are regions where there is very little cloud, so simulations with more extensive cloud in these marginal regions, along with less PI CCN (and sulfur) to maintain clouds in mid-latitudes, yield larger net ACI response. The strong opposite sign of the high latitude correlations as noted are likely due more to the change in ACI components over the Arctic than changes in the mean state.

We can also look for which parameters give rise to the largest sensitivity in changes between pre-industrial and present day. Parameters affect particular processes, so we can use parameter sensitivity as a means to focus on particular processes or sets of processes. Since the PPE spans parametric uncertainty, this analysis identifies the sensitivity of processes to parametric uncertainty, and the impact of those processes on forcing and feedback. For example, parameters for auto-conversion and accretion alter the rain formation process which is the main sink for cloud water (regulating LWP).

Following Eidhammer et al. (2024), we examine changes in model state (PD - PI) as a function of parameter in Figure 5. The parameter values (y-axis) are normalized (scaled by the minimum and maximum parameter values) while the differences in the outputs (x-axis) are standardized (scaled by the mean and standard deviation of the output values) and then regression slopes are calculated for global and regionally averaged values. Figure 5 illustrates the slopes for the normalized regression. The normalization and standardization helps show which parameters drive PD-PI changes in each output. Parameters are listed by parameterization and the regressions are calculated for different latitude bands as well as global. There are many commonalities across regions, with the exception being that cold cloud parameters are more important in the tropics and mixed phase cloud parameters are important in the Arctic. Given that ACI forcing is mostly in the N. Hemisphere, we do not expect any strong relationships over the Southern Ocean.

Important parameters for ACI changes (PD - PI mean quantities) are concentrated, not surprisingly, in the cloud microphysics and aerosol activation parameterizations since ACI processes trace aerosol changes, effects on cloud drop number and cloud microphysical adjustments to drop number perturbations. Total aerosol forcing (ACI and direct radiative effects of aerosols) is expressed in the residual TOA flux (RESTOM) difference, and the cloud forcing (SW CRE and LW CRE are the PD - PI change in these quantites). Important parameters alter both accretion ($micro\_mg\_accre\_enhan\_fact$) and auto-conversion ($micro\_mg\_autocon\_lwp\_exp$ and $micro\_mg\_autocon\_nd\_exp$): the main loss process for cloud liquid water. In the Arctic, the threshold size of ice crystals for conversion of ice to snow ($micro\_mg\_dcs$) is important for ice cloud effects, including changes in ice cloud mass and the changes in both LW and SW CRE (LWCF, SWCF). Ice fall speed ($micro\_mg\_vtrmi\_factor$) is also important globally. The scaling of the sub-grid vertical velocity for ice nucleation ($microp\_aero\_wsubi\_scale$) is important in the tropics and globally for governing the ice number and hence the LW and SW radiation. Note that it does not impact the net TOA balance change because of the offsetting SW and LW effects. The sub-grid vertical velocity for liquid drop activation ($microp\_aero\_wsub\_scale$) is also important. Liquid drop activation affect CCN formation. In the mid-latitudes, including the regions over the ocean where thicker PI clouds increase ACI magnitude, several of the turbulence parameters from CLUBB are important.

To take this a bit further, we can break down some of the key correlations in Figure 5 by correlating parameter values and net ACI forcing at each point. As in Figure 4, we estimate significant correlations with a bootstrap fit. We then determine the global average mean absolute correlation from only the location of significant correlations. Figure 6 illustrates the mean absolute correlation for each parameter for 6 different forcing and feedback components (different colors): Total, LW and SW for ACI and Cloud Feedback. The squares in Figure 6 show the

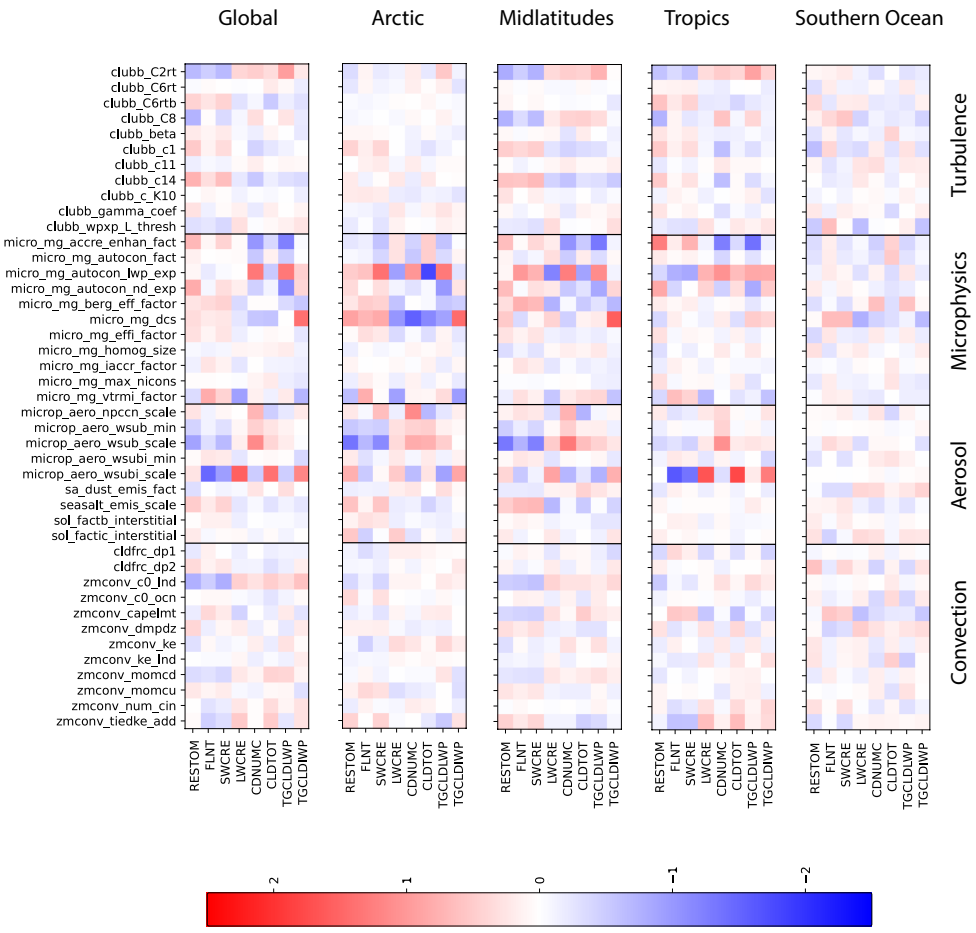

Figure 5. Normalized linear regression slope for the difference between PD and PI in 8 different model outputs (x axis) against all parameter values (y axis). The global mean results as well as four different regions are shown; Arctic ($|lat|> 60°$), Midlatitudes ($30°<|lat|< 60°$), Tropics ($|lat|< 30°$) and the Southern Ocean ($60°\text{S}>lat>30°\text{S}$). The parameters are grouped into deep convection, aerosol, microphysics and turbulence parameters.

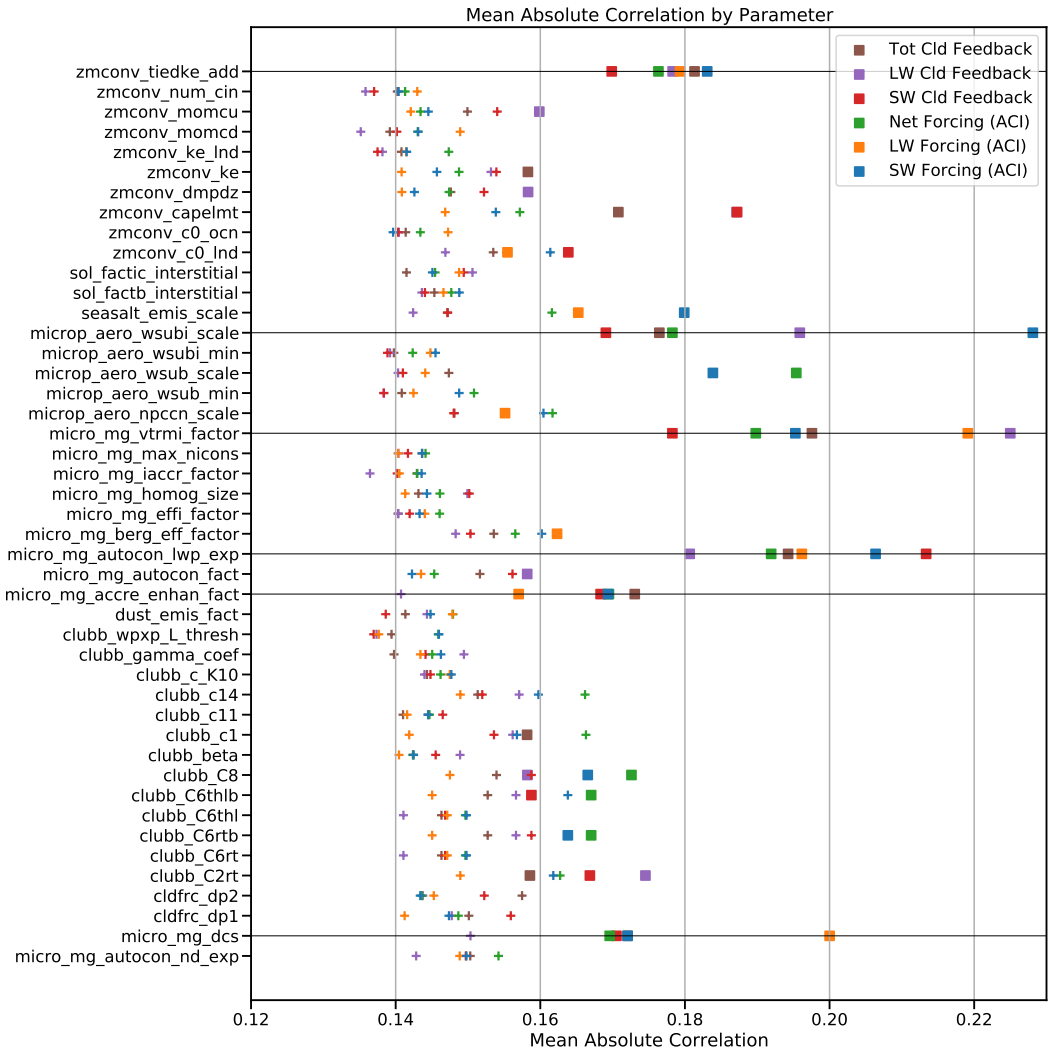

Figure 6. Global mean absolute correlation by parameter for ACI Forcing and Cloud Feedbacks. LW, SW and Net are different colors as noted in the legend (e.g. net ACI forcing is green). Parameters with the 10 highest absolute correlations for each component are shown as colored solid squares. The rest of the parameters are plus signs (+). The horizontal lines show the 6 parameters which are in the top 10 correlations for both total cloud feedback (brown) and net forcing (green).

parameters with the 10 highest correlations for each component. We will focus on the common important parameters across forcing and feedback (horizontal lines) in Section 3.4.

Focusing on the net ACI Forcing (green in Figure 6), we highlight the parameters with the 10 highest mean absolute correlations (green squares). In general the LW (orange) and SW (blue) forcing components also have strong correlations with these parameters. Figure 7 illustrates maps of these correlations, ranked as in Figure 6 in order of correlation from highest (A) to 10th highest (J).

Figure 7 reinforces the global and regional correlations in Figure 5, with a bit more insight into processes. Several parameters are related to ice, including the

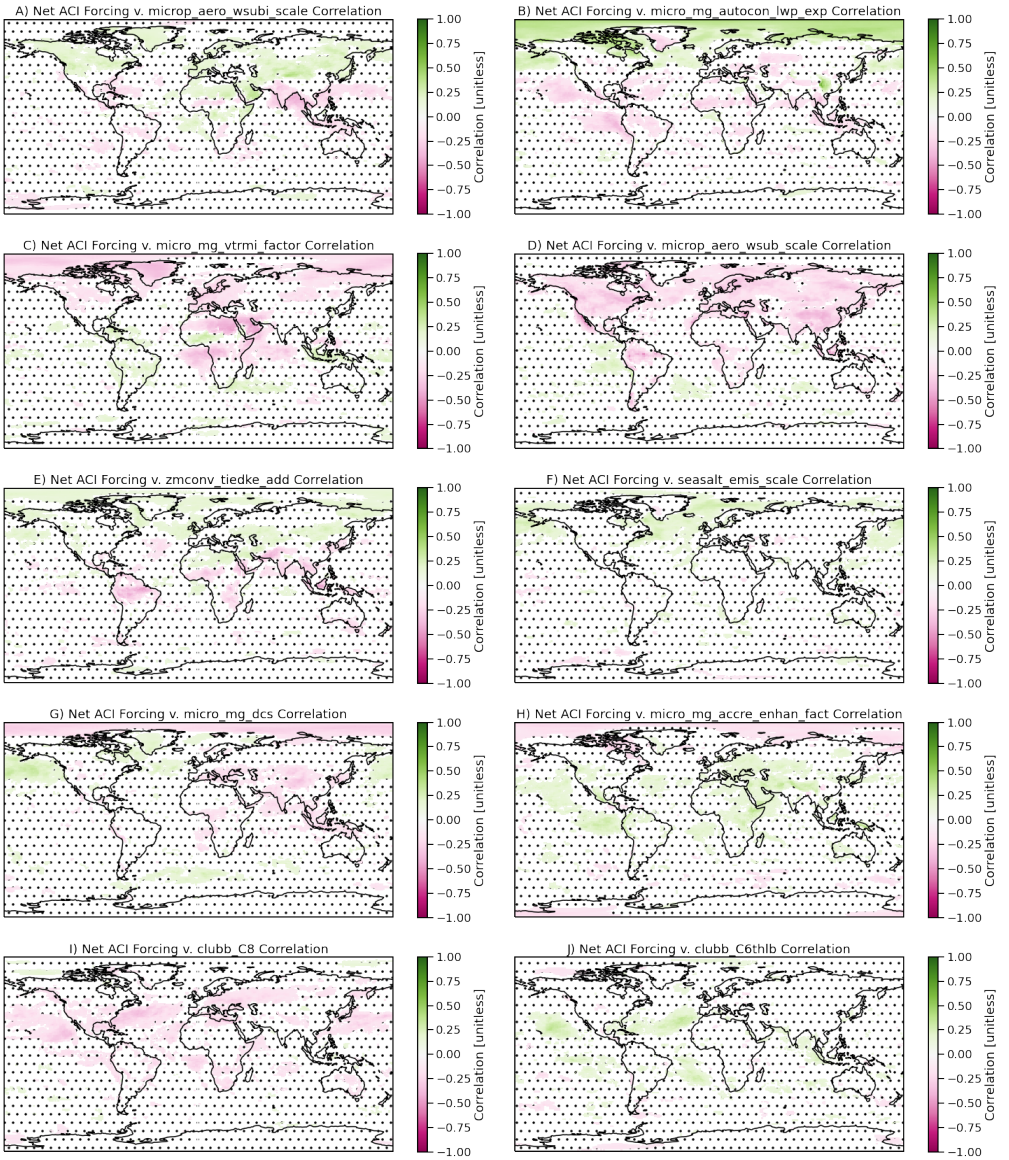

Figure 7. Map of linear correlation coefficient at each point between the SW ACI forcing (PD-PI) and selected model parameters varied in the PPE. Non-significant points are stippled. Significance is determined by a bootstrap fit.

sub-grid velocity for ice activation (*micro_aero_wsubi_scale*: Figure 7A), the ice fall speed scaling (*micro_mg_vtrmi_scale*: Figure 7C) and the ice auto-conversion size threshold (*micro_mg_dcs*: Figure 7G). The temperature perturbation for deep convective triggering (*zmconv_tiedke_add*, Figure 7E) likely also plays a role in supplying ice to the upper troposphere. Increasing the sub-grid velocity for ice nucleation will increase ice number (which seems to weaken ACI over land). The ice fall speed scaling results in less ice and snow in the atmosphere (associated with stronger ACI), while increasing the ice auto-conversion size threshold will increase the ice mass, which seems to weaken ACI in mid-latitudes but increase it at high latitudes (so more ice will result in stronger ACI at high latitudes, consistent with the PI mean state IWP relationship in Figure 4C).

Liquid cloud processes are also important. The auto-conversion LWP exponent (*micro_mg_autocon_lwp_exp*: Figure 7B) and accretion enhancement factor (*micro_mg_accre_enhan_fact*: Figure 7H) control rain formation and depletion of liquid. They have similar patterns and opposite sign. Increasing the LWP exponent for auto-conversion results in more sensitivity of cloud water loss to LWP: higher auto-conversion sensitivity in the subtropics in results in stronger (more negative) ACI, while higher auto-conversion sensitivity in the Arctic results in weaker (less negative) ACI. Accretion is also a sink for cloud water, and the enhancement is a linear scaling for the loss. In the sub-tropics, more accretion leads to reduced (negative) ACI, and would be associated with thinner clouds. The accretion scaling is consistent with the sensitivity of ACI to PI mean state sensitivity of clouds in Figure 4, while the auto-conversion exponent is more related to the changes in the state between PI and PD.

Two parameters are related to liquid aerosol activation: increasing *microp_aero_wsub_scale* (Figure 7D) is associated with larger negative ACI. Higher scaling would increase CCN in PI, but also the sensitivity to changes between PI and PD (ΔCCN). Given that the correlation with ACI in Figure 7D is opposite to the mean state effect of PI CCN in Figure 4E, it would appear that it affects ACI more through ΔCCN. Increasing sea salt emission (*seasalt_emis_scale*), will increase CCN in the base state, and has a similar correlation with ACI as PI CCN (Figure 4E) over the oceans.

The last two parameters are related to the unified shallow turbulence (CLUBB) and act over the sub-tropical oceans. *clubb_C*8 (Figure 7I) is the coefficient of the skewness in the vertical velocity while *clubb_C*6*thlb* (Figure 7J) affects the high skewness of the liquid water potential temperature. They tend to act in opposite ways. Increasing *clubb_C*8 tends to increase cloud fraction, so the correlation matches the total cloud response in Figure 4A.

Looking beyond the mean state, we can also try to understand how ACI is related to the sensitivity or susceptibility of cloud radiative effects to changes in cloud properties. To look at this we examine the susceptibility of cloud radiative effect (or cloud albedo) to changes in cloud drop number (Nc) defined as dln(Albedo)/dln(Nc). We estimate the susceptibility terms at each point with the temporal (monthly mean) co-variance of these properties for each ensemble member, and then similar to Figure 4, correlate that with the total ACI (difference in LW+SW CRE between PD and PI) in Figure 8A. Because albedo has a strong seasonal dependence at high latitudes, we limit this analysis to latitudes equatorward of 60°.

There is a consistent negative correlation between susceptibility and forcing over the oceans, whereby increasing susceptibility of clouds to drop number is associated with stronger negative net ACI over the tropical and sub-tropical oceans. A detailed analysis of the parameter sensitivity of susceptibility (not shown) sim-

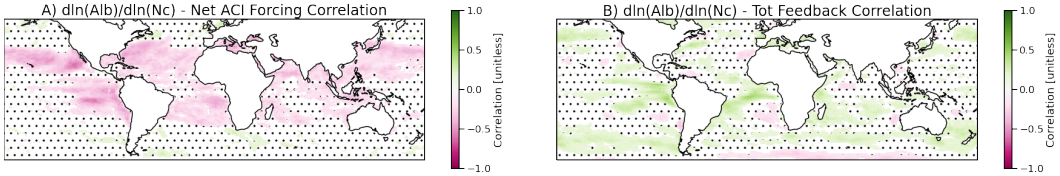

Figure 8. Correlation of susceptibility of cloud albedo to cloud drop number against A)Net ACI forcing and B) Total Cloud feedback.

ilar to that conducted for Figure 7 for forcing indicates that the susceptibility is linked to the auto-conversion (*micro_mg_autocon_lwp_exp*) where more susceptible clouds have a higher auto-conversion exponent for LWP (interestingly it is not related as much to the Nc exponent in the auto-conversion). In addition, susceptibility varies with accretion (*micro_mg_accre_enhan_fact*), where more accretion reduces susceptibility (perhaps because of thinner clouds). Finally, susceptibility is also associated with *clubb_C*8, where higher *clubb_C*8 is associated with higher susceptibility. H. Guo et al. (2015) noted that increasing *clubb_C*8 increases cloud cover in the subtropics. These results are consistent with the PI mean state correlations (Figure 4) that thicker sub-tropical PI clouds in marginal regions are associated with higher (negative) net ACI forcing.

3.3 Feedback

A similar analysis is conducted for cloud feedbacks. Cloud feedbacks are assessed with the difference in cloud radiative effects between the SST+4K and PD simulations (modified with radiative kernels to remove non-cloud effects). Because global correlations can be misleading with positive and negative signs and cloud feedbacks have multiple signs in different regimes (Figure 2), we move straight to correlations with the mean present day state and total (LW+SW) cloud feedbacks at each point in Figure 9. These figures are with respect to present day values, but the correlations are the same whether present day or pre-industrial mean state is used. Figure 9 includes all simulations, but is qualitatively consistent with less significance if the 88 simulations constrained by CERES cloud radaitive effect are used.

Regional correlations between cloud feedbacks and mean state cloud coverage (Figure 9A) are negative at high latitudes (Arctic and Southern Ocean) and positive at low latitudes. The correlations over the Sahara are spurious since there is nearly zero cloud and feedbacks are small (Figure 2C). Similar relationships are found with LWP (Figure 9B), cloud drop number (Figure 9J) and cloud top number (Figure 9I). Base state SW Cloud Radiative Effect (Figure 9G) has an opposite sign correlation (because it is negative) with similar pattern. However, over the Southern Ocean, more cloud and LWP (more liquid cloud) has a negative correlation with cloud feedbacks. IWP (Figure 9C) however has positive correlations over polar oceans. Base state ice fraction (Figure 9H) is positively correlated with total cloud feedbacks as well at high latitudes, and negatively correlated at low latitudes. All these correlations indicate that at high latitudes stronger cloud feedbacks are associated with less base state cloud, liquid and liquid drop number, as well as more ice. Note that as with forcing, the net feedback sign changes at high latitudes, which affects these correlations (the same change in mean state has a different sign with different signed feedbacks). In low latitudes, the effects are opposite, with stronger feedbacks for more and thicker cloud over land and ocean. There are weaker relationships between feedbacks and column sulfate (Figure 9D) and CCN (Figure 9E), but in general

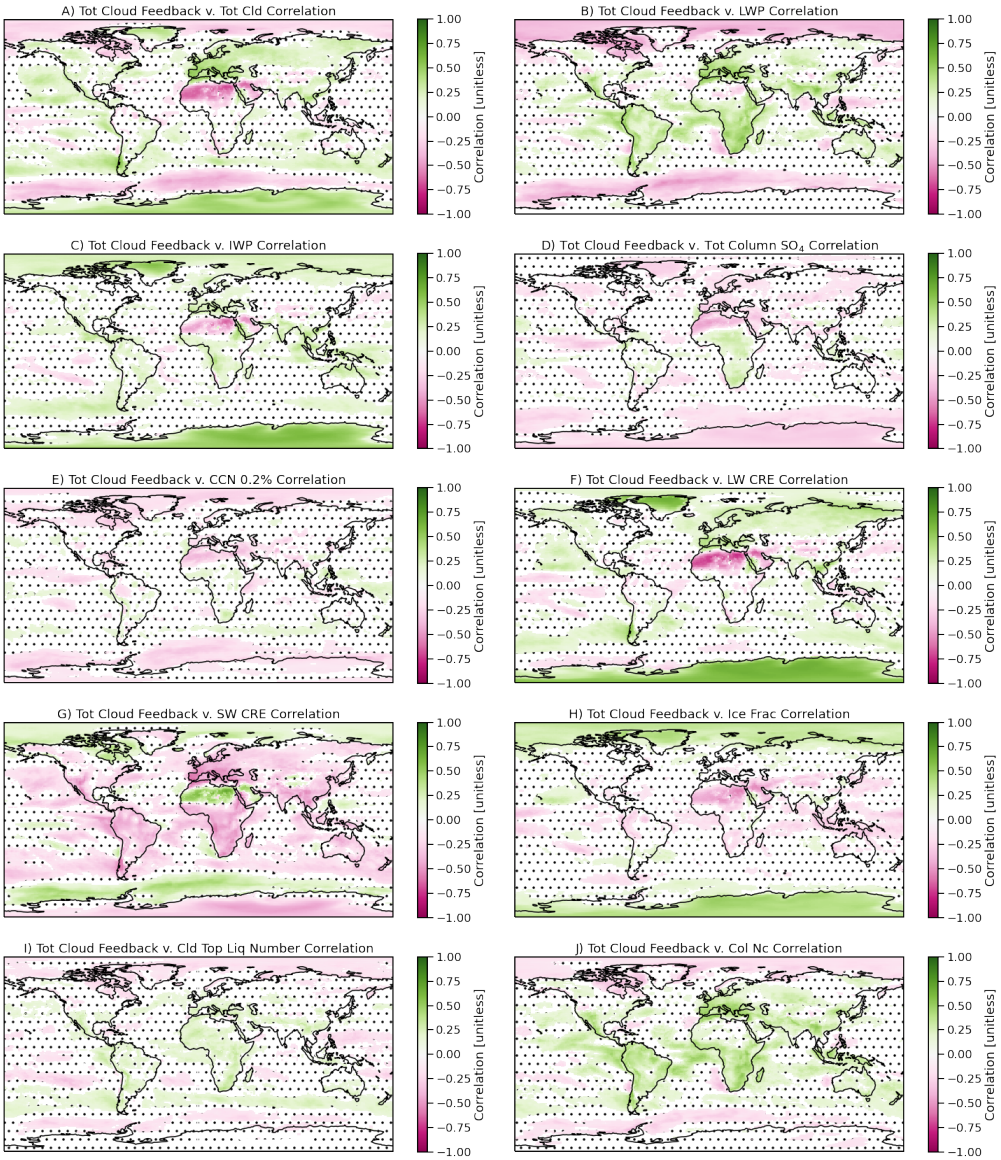

Figure 9. Map of linear correlation coefficient at each point between mean state in present day and the total (LW+SW) cloud feedbacks (estimated with SST4K v. PD) for different variables. Non-significant points are stippled. Significance is determined by a bootstrap fit.

more sulfate and CCN in the base (non-warmed) state is associated with lower feedbacks.

We investigate these relationships further by diving into processes by looking at key parameters. Figure 10 is similar to Figure 5 showing the normalized and standardized regressions between parameters and changes in the state SST4K - PD across regions. Some of the same parameters are important for cloud feedbacks (the last two variables on the right of each column): accretion, auto-conversion and the loss process of ice (fall speed and conversion from ice to snow). Note that the S. Ocean is not important for forcing since there is little change in aerosols PD-PI, but is more important for feedbacks (accretion, ice processes and some deep convection parameters are important here). As with the maps in Figure 9, the correlations vary by region, muting the global sensitivity (correlation) for many parameters.

There are several parameters in the deep convective parameterization that are important for cloud feedbacks, particularly in the Tropics and to a lesser extent the S. Ocean. These parameters govern the triggering of convection (*zmconv_capelmt* is the threshold CAPE for firing convection and *zmconv_tideke_add* is a buoyancy perturbation that will increase the convective potential). Convective rain formation over land (*zmconv_c0_lnd*) is also important in the tropics, which is not surprising given the larger positive cloud feedbacks there (Figure 2). Convective entrainment (*zmconv_dmpdz*) is important in the mid-latitudes and tropics. Deep convection acts by changing both the SW and the LW feedback, likely because it changes ice cloud radiative effects, while many of the other parameters primarily change the LW (for ice microphysical and aerosol processes) or SW (for liquid cloud microphysical and aerosol processes).

Finally for we look at maps of key parameter correlations with feedbacks in Figure 11. As with Forcing, we estimate the mean absolute correlation of significant points for each parameter, and rank them (Figure 6). The parameters with the 10 highest correlations with total feedbacks (brown squares in Figure 6) are displayed in Figure 11.

The parameters identified are similar to those for forcing. There are several parameters linked to ice processes, including ice fall speed (*micro_mg_vtrmi_scale*, Figure 11A), the sub-grid velocity for ice activation (*micro_aero_wsubi_scale*: Figure 11D) and the ice auto-conversion threshold (*micro_mg_dcs*, Figure 11F). Slower fall speed and more ice number (higher *micro_aero_wsubi_scale*) at high latitudes are associated with more ice and higher total cloud feedbacks at high latitudes (Figure 9C). Ice auto-conversion (*micro_mg_dcs*) acts mostly in the tropics and S. Hemisphere, again with more base state ice (higher *micro_mg_dcs*) associated with higher cloud feedback, likely through the LW CRE (Figure 9F).

As with forcing, parameters linked to rain formation are important for cloud feedbacks, the auto-conversion LWP exponent (*micro_mg_autocon_lwp_exp*, Figure 11B) and accretion enhancement (*micro_mg_accre_enhan_fact*, Figure 11E) have opposite signs. Higher auto conversion (leading to less liquid) is associated with smaller cloud feedbacks at high latitudes and larger cloud feedbacks at lower latitudes. Accretion has the opposite effect, with more accretion (reducing cloud water) associated with more high latitude cloud feedbacks, and reduced tropical cloud feedbacks over land. Both effects are consistent with the overall cloud and LWP correlations with feedbacks in Figure 9A and B.

In addition, there are three deep convective parameters that have regionally significant correlations with cloud feedback. In the tropics, deep convection supplies ice to the upper troposphere, *zmconv_tiedke_add* (Figure 11C) as well as *zmconv_ke* (Figure 11I) increase convection over land with similar patterns. *zmconv_capelmt*

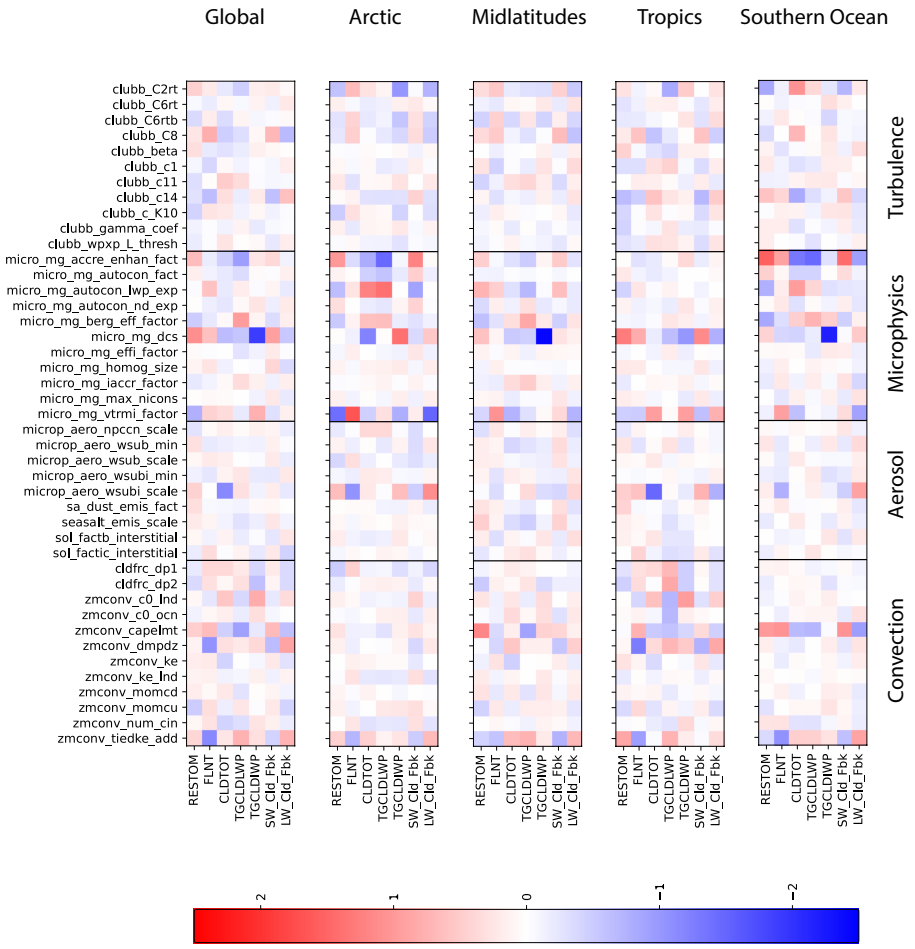

Figure 10. Normalized linear regression slope for the difference between SST4K and PD in 8 outputs (x axis) against all parameter values (y axis). The global mean results as well as four different regions are shown; Arctic, Midlatitudes, Tropics and the Southern Ocean. The parameters are grouped into deep convection, aerosol, microphysics and turbulence parameters.

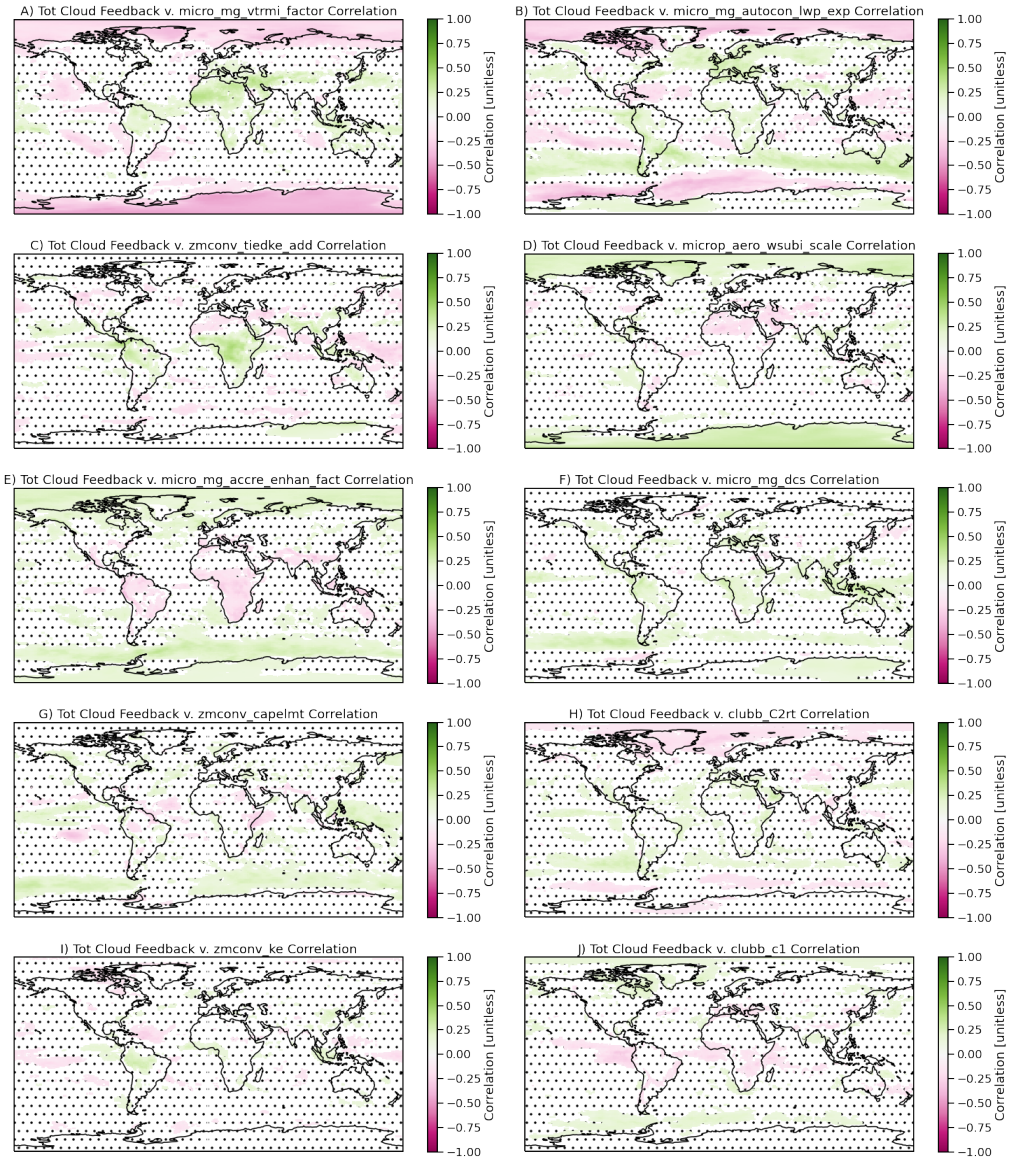

Figure 11. Map of linear correlation coefficient at each point between the total cloud feedbacks (SW + LW) estimated from SST4K v. PD and selected model parameters varied in the PPE. Non-significant points are stippled. Significance is determined by a bootstrap fit.

(Figure 11G) increases it over ocean. Increasing ice seems to increase cloud feedbacks in the tropics (Figure 9C). *zmconv_capelmt* (Figure 11G) also seems to act over the Southern Ocean, with offsetting signs in the LW and SW (Figure 10).

Finally, two turbulence parameters, *clubb_C2rt* (Figure 11H), *clubb_c1* (Figure 11J) have small regional correlations, mostly over the oceans with opposite sign. *clubb_C2rt* is related to the dissipation of temperature variance and increasing it increases cloud cover and SW CRE (Z. Guo et al., 2015) while *clubb_c1* is related to the dissipation of vertical velocity variance and has the opposite effect (increasing it decreases cloud cover and SW CRE). The patterns indicate that these parameters may be driving some of the correlation with mean state total cloud cover and LWP (Figure 9A and B), in both the tropics and high latitudes.

3.4 Forcing and Feedback Relationships

Figure 12 illustrates a global scatter plot of the cloud forcing (defined as above: the change in CRE between present day and pre-industrial) against the kernel adjusted cloud feedbacks both in the SW (Figure 12A), LW (Figure 12B) and total (LW+SW, Figure 12C). The blue colors and regression line are for all simulations. As in Figure 12, the orange points and regression lines are just those simulations whose mean annual value of SW CRE is within ± 5 Wm^{-2} of the observed CERES EBAF annual global mean (-45.3 Wm^{-2}). The red dot is the 'default' parameter set for CAM6.

In the SW, there is a clear relationship between the cloud feedbacks and cloud forcing. The relationship is similar whether just a constrained subset of simulations is used, or if the full data set is used, and the slope is significantly different that zero. In general the SW aerosol cloud forcing is negatively correlated with SW cloud feedback: larger positive feedbacks yield larger negative cloud forcing. There is no such correlation in the LW, and the slopes are not significantly different than zero, and the constrained simulations have a different (but still not significant) sign. The correlation of total (LW+SW), cloud forcing and feedback reflects mostly the SW correlation, and is actually stronger with constrained simulations.

As with forcing and feedback, we can decompose the global correlation of Figure 12 into each location on the planet, generate a correlation value at each point, and determine the significance of the correlation with a bootstrap fit yielding a confidence interval for the correlation between forcing and feedbacks being significantly different than zero (Figure 13) at each point. For the SW (Figure 13A), correlations are uniformly negative: stronger negative ACI is correlated with stronger positive cloud feedback. This maximizes over N. Hemisphere land and adjacent ocean basins. In large parts of the S. Hemisphere, there is very little forcing response, so there are small signals. Most of the negative correlation comes from the N. Hemisphere. Going back to the regional correlations between mean state SW CRE and ACI (Figure 4G) and total cloud feedbacks (Figure 9G), there is an anti-correlation, consistent with stronger forcing and feedbacks going together (since forcing is negative), with opposite signs over the Arctic and the rest of the N. Hemisphere. It is apparent over both ocean and land.

For the LW (Figure 13B), the sign is not monotonic, but there is a negative correlation in N. Hemisphere mid-latitudes, and a positive correlation between LW feedbacks and LW forcing (which are generally both of the same positive sign) in parts of the tropics and the Arctic, but with less significance. The patterns of LW forcing and feedbacks (shown in Figure 2) are less correlated than the SW, likely since the SW ACI magnitude and processes acting through liquid are stronger than for ice. Indeed, if we look at changes in the different climate states between forcing (PD - PI) and feedback (SST4K - PD), the strongest negative correlations are

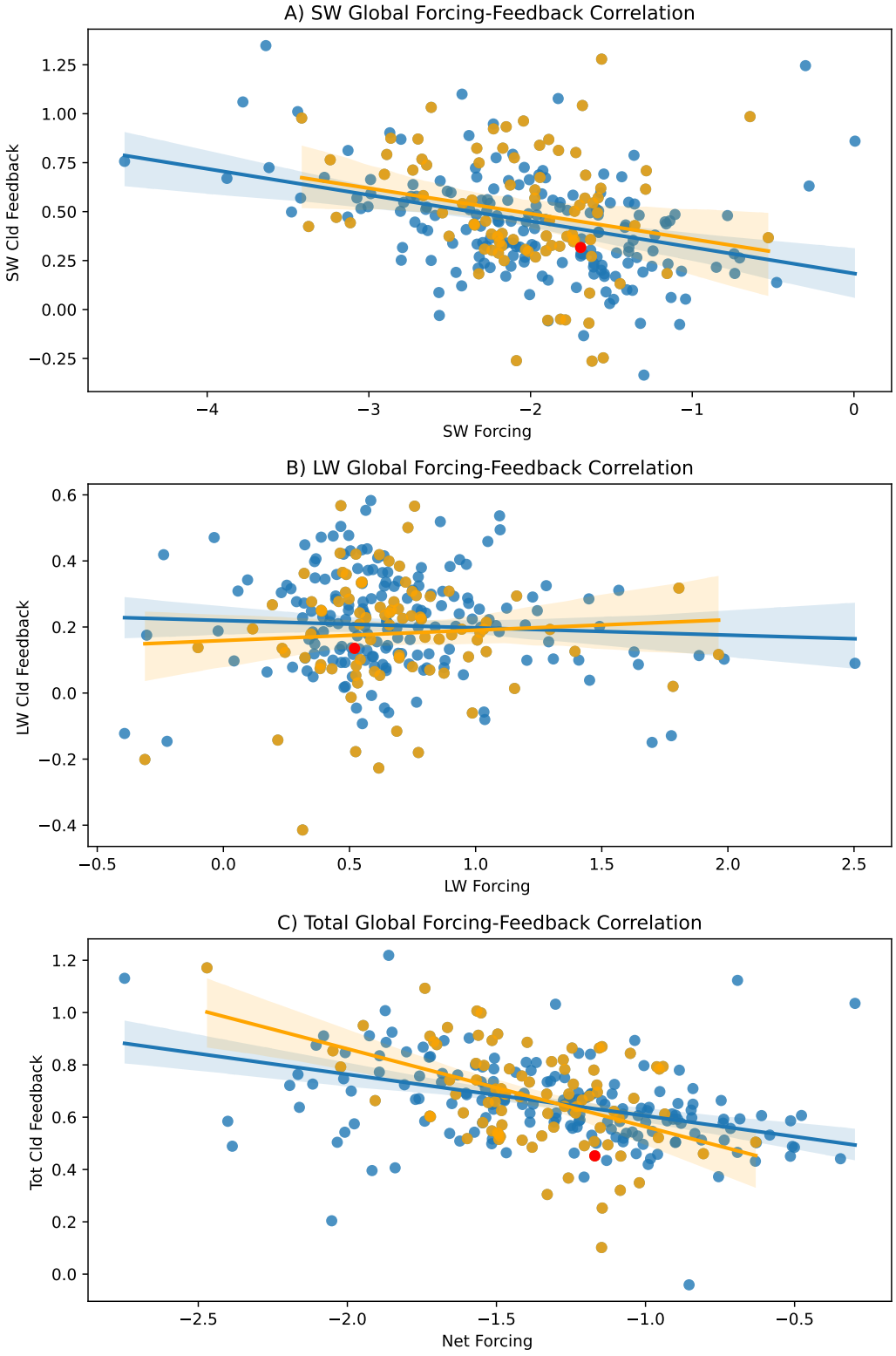

Figure 12. Scatterplot of A) SW B) LW and C) Total (LW+SW) Aerosol forcing (horizontal axis) and kernel adjusted cloud feedbacks (vertical axis) from each simulation. Orange indicates those 88 simulations whose global mean PD Shortwave Cloud Radiative Effect is within ±5 Wm^{-2} of the CERES EBAF global annual mean. Default CAM6 parameters shown as the red dot.

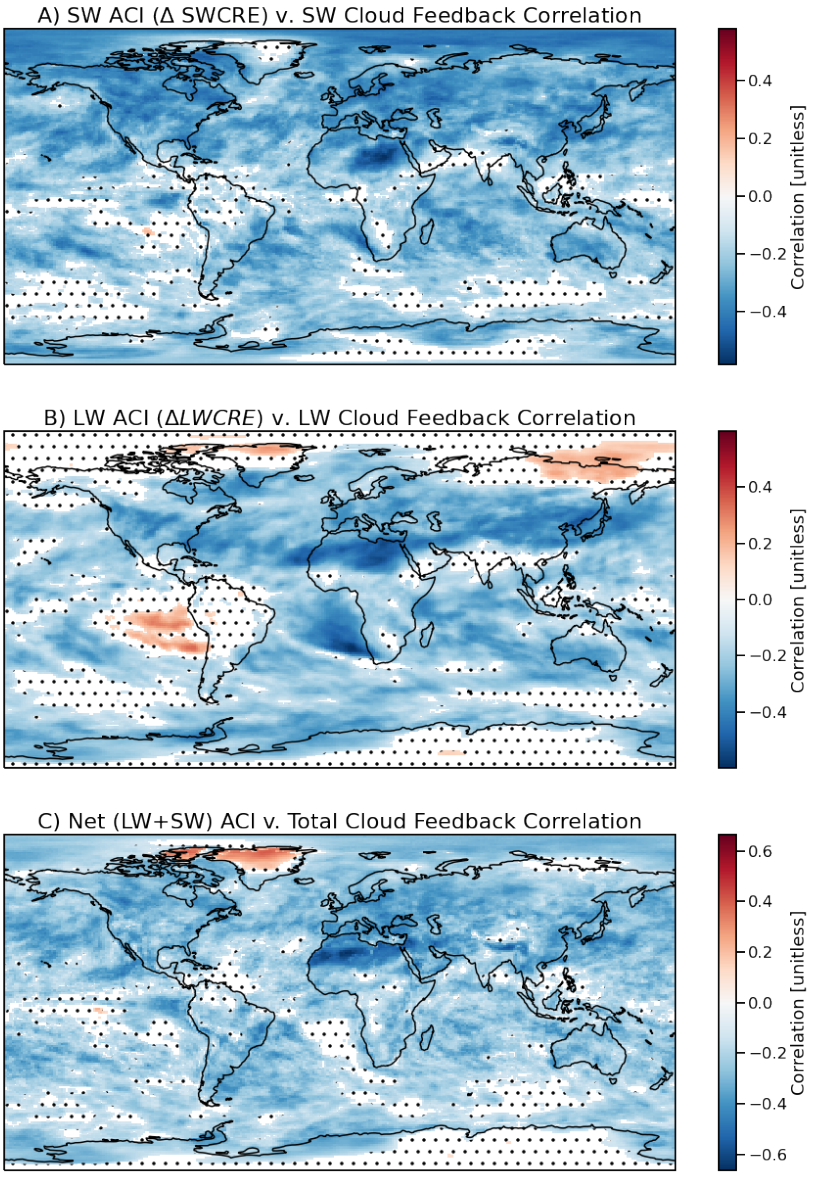

Figure 13. Correlation maps at each point between A) SW, B) LW and C) Total (SW+LW) Cloud Forcing and Feedback. Regions of less than 95% significance are stippled.

with N. Hemisphere mid-latitude LWP and column drop number (Figure B1), which affect mostly SW radiation. The correlations between net forcing and feedbacks (Figure 13C) are lower than the SW, but also negative.

There is also a positive relationship between cloud albedo susceptibility to drop number and cloud feedbacks (Figure 8B). The correlation is the opposite as for ACI forcing, which may be another reason for the anti-correlation between forcing and feedback. Increased susceptibility (through the processes described above under forcing), tends to create larger magnitude negative ACI forcing and positive cloud feedbacks.

Finally, we note that some of the dominant parameters governing Forcing and Feedbacks are similar. Using the mean absolute correlations by parameter (Figure 6), we determined the most relevant parameters for ACI forcing in Figure 7 and cloud feedbacks in Figure 11. Figure 6 illustrates that of the top 10 correlations between parameters and forcing and feedback, 6 of them are common (horizontal lines). These include 3 parameters for ice: ice fall speed (*micro_mg_vtrmi_scale*), ice nucleation sub-grid velocity (*microp_aero_wsubi_scale*) and ice to snow conversion size threshold (*micro_mg_dcs*). There are two parameters related to warm rain formation, one each for auto-conversion (*micro_mg_autocon_lwp_exp*) and accretion (*micro_mg_accre_enhan_fact*). One parameter is related to the triggering of deep convection (*zmconv_tiedke_add*).

To illustrate how the co-variation of these parameters affect forcing and feedback, we build a Gaussian process emulator using the global average forcing and feedback. Inputs are the normalized parameter values and global net forcing and total feedbacks (LW+SW). Figure 14 illustrates how global mean total cloud feedbacks and net ACI forcing vary around the default values as these parameters change individually based on the emulator. The emulator is not a perfect representation of the total 45 dimensional parameter space, and it is built on global values (with attendant problems of different responses by regime), but it is illustrative of another method to understand the interaction of forcing and feedback.

In this emulator, some parameters affect only either feedbacks (ice conversion threshold: *micro_mg_dcs*) or forcing (ice fall speed: *micro_mg_vtrmi_factor*), and some affect virtually neither in the emulator (deep convective triggering: *zmconv_tiedke_add*). This might be because the global positive and negative correlations cancel. Ice nucleation sub-grid velocity (*microp_aero_wsubi_scale*), which changes ice crystal number is weakly non-linear, while auto-conversion (*micro_mg_autocon_lwp_exp*) and accretion (*micro_mg_accre_enhan_fact*) parameters have complex relationships and act differently for feedback, but similarly for forcing. Such emulators can be used as a further guide for understanding the slices through the parameter space. The opposite effects on feedbacks of auto-conversion and accretion are consistent with correlations in Figure 11 for example. For forcing, the different magnitudes of negative and positive responses (Figure 7) may make emulating the global mean difficult.

4 Discussion

We can summarize this analysis with several comments about key processes for forcing, feedbacks and their interaction in the CAM6 PPE.

4.1 Forcing

Stronger negative ACI forcing is associated with PI climates that have thicker, more extensive clouds with higher drop numbers and water path in the subtropics.

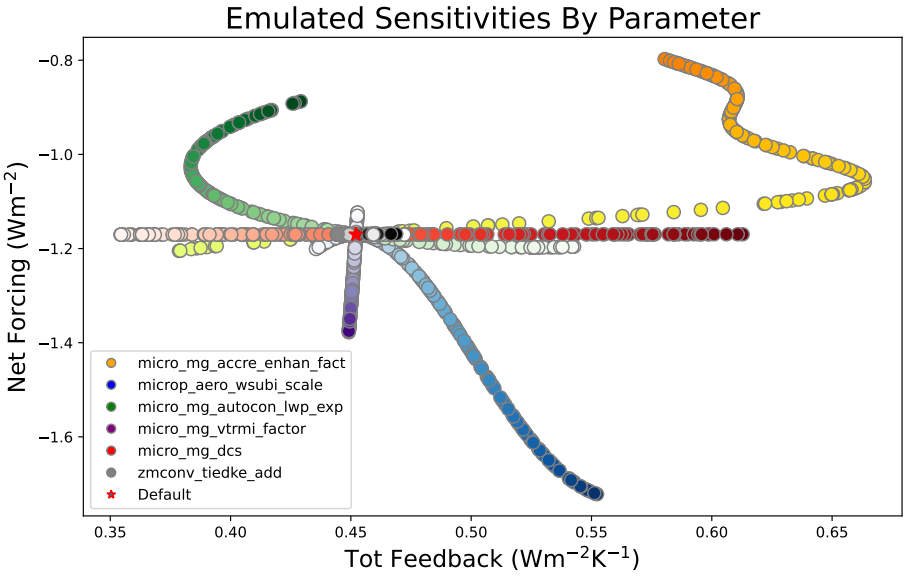

Figure 14. Sensitivities by parameter using the Gaussian Process emulator. Top common parameters are shown, varied around the default location (marked with a red star). Color hue varies from light (0) to dark (1) of the normalized range.

The regions in the sub-tropics that are most sensitive to parameter changes are regions where there is very little cloud, so simulations with more extensive cloud in these marginal regions, along with less PI CCN and sulfur, seem to yield larger net ACI. This highlights that the pre-industrial state of clouds is important for ACI, as noted by Carslaw et al. (2013) and others.

Auto-conversion and accretion are critical processes. Auto-conversion and accretion parameters that lead to increased cloud thickness in the subtropics increase negative ACI (consistent with mean state effects). Increasing activation with increased sub-grid vertical velocity leads to stronger negative ACI nearly everywhere (more response to aerosols, more change in CCN, since lower CCN in PI are associated with stronger ACI). Increasing sea salt emission (which increases PI and PD CCN similarly) reduces net ACI, because it means more CCN in PI (consistent with the interactions with the mean state). Correlations with changes to the auto-conversion LWP exponent seem larger than for accretion, but accretion is scaled linearly, and the variations on the auto-conversion are larger (there is also a linear auto-conversion scaling parameter which does NOT show up as being significant). Accretion affects ACI through PI mean state (thicker clouds yield larger magnitude ACI), while auto-conversion affects ACI through the sensitivity of PD-PI differences in LWP.

Increasing susceptibility of cloud albedo to drop number increases negative ACI forcing, over much broader regions than a single parameter or mean state property. Susceptibility is driven by a slightly different set of parameters, including auto-conversion and accretion, but also shallow turbulence parameters that increase cloud cover in the sub-tropics, again, in regions where it is generally low.

4.2 Feedbacks

In low latitudes, stronger positive cloud feedbacks are associated with more base state cloud, liquid and liquid drop number, as well as more ice over land and ocean. More ice (and higher ice fraction) at high latitudes increases cloud feedback, while correlations for liquid are the opposite (more liquid is associated with more negative cloud feedback). There is a dipole in these effects over the S. Ocean where the mean ice fraction crosses about 50%. This is related to the loss processes for water (auto-conversion and acccretion) as well as for ice (ice fall speed and ice activation), and the deep convective source for ice. It is near the region where feedbacks turn from positive to negative. In ice dominated regions feedbacks are negative likely due to the ice-albedo feedback, whereby warming melts ice and increases negative SW CRE. This has been shown to be important in CAM6 (Gettelman et al., 2019).

Going strictly by the correlations, it appears that that auto conversion is more important (or at least more related to) the base state cloud feedback sensitivity than accretion (correlations for accretion are weaker). Raining and non-raining clouds may have different effects, with perhaps the non-raining clouds more important for feedback. Turbulence parameters also seem to play a role over the sub-tropical oceans: they control the base state of clouds and thicker and more extensive clouds have more positive cloud feedbacks. More ice yields stronger positive cloud feedbacks (mostly through the LW) in both the tropics and high latitudes. Ice microphysics and deep convection parameters are important for regulating ice mass and seem to influence feedbacks accordingly.

4.3 Interactions

Forcing and feedbacks are anti-correlated throughout the Northern Hemisphere. Both forcing and feedback relationships to the mean state change sign from high latitudes to lower latitudes, and they seem to do so in concert. Part of this is simply the reduction in SW effects over high latitude ice covered surfaces. Stronger negative forcing and positive feedbacks are associated with thinner clouds (less liquid, more ice) at high latitudes and thicker clouds at low latitudes. This change may occur because of the role of ice process, or the thickness of the clouds in the stormtracks.

Even the important processes seem to be common between aerosol forcing and cloud feedbacks. Microphysical controls on ice and ice nucleation, rain formation (auto-conversion and accretion) as well as deep convection are important for both forcing and feedback, with some shallow turbulence parameters (but different ones) important over the oceans. Most of these parameters seem to be consistent with sensitivity in the mean state.

One question arises: given that changing the method for auto-conversion and accretion drastically (e.g., Gettelman et al., 2021) did not change ACI or cloud feedbacks, how does that mesh with these results? We have not tested changing auto-conversion and accretion fundamentally and altering other parameters, but it may be that the balance required to maintain the mean state clouds constrains the range of ACI and cloud feedbacks. This is consistent with the correlations with the mean state of clouds, and would imply an emergent constraint dependent on the present day state, but perhaps not a strong constraint.

5 Conclusions

This analysis of a large ensemble set of perturbed parameter experiments from CAM6 (CAM6-PPE) yields several conclusions. Forcing and feedback are both cor-

related with the mean state. Higher magnitude cloud radiative effects generally mean larger forcing (negative for the SW, positive for the LW) and larger feedbacks (positive SW and LW). Aerosol forcing is broadly related to the susceptibility of clouds to drop number, which is impacted by a similar set of parameters, but with a different magnitude.

For aerosol forcing in particular, lower PI CCN and sulfate mass yield higher magnitude forcing. Accretion affects the mean state (and the total water mass in clouds), while auto-conversion seems to affect the sensitivity of LWP more strongly.

Thicker low latitude clouds with higher susceptibility are also associated with more positive cloud feedbacks. At high latitudes stronger positive cloud feedbacks are associated with less base state cloud, liquid and liquid drop number, as well as more ice at high latitudes. The shift happens about where ice starts to dominate the cloud (50% ice fraction). The fact that many important parameters reflect ice processes confirm the importance of ice in CAM6 feedbacks.

Aerosol forcing and cloud feedbacks are not independent in the CAM6 PPE, they are anti-correlated, such that stronger negative forcing is associated with stronger positive feedbacks. The fact that both forcing and feedbacks change sign in high latitudes of the N. Hemisphere at the same latitude is likely due to the LW and SW balance changing over an ice covered surface.

Even the processes governing forcing and feedback sensitivity in the PPE seem to be similar. The warm rain formation process (auto-conversion and accretion), ice loss processes (activation, fall speed, auto-conversion to snow) and deep convective intensity (which affects ice) are important for both forcing and feedbacks. Using these processes, it is possible to build emulators for forcing and feedbacks to try to understand the sensitivities.

This process-based view shows that in a consistent model system there are relationships between aerosol forcing and cloud feedbacks. Such relationships may be representative across multi-model ensembles as has been seen in the past (Kiehl, 2007; Forster et al., 2013), but not necessarily given the small sample size (Smith et al., 2020).

This detailed analysis of cloud processes and their interactions with parameters to yield forcing and feedback sensitivities has yielded new insights into CAM6. But this is only one model of many different climate models, with a unique and complex representation of cloud processes. How applicable is this result across a range of models? Similar PPE methods should be and are being performed with other models. Some aspects of this analysis should have broad applicability. For example, the parameterizations used in CAM6 for deep convection (G. J. Zhang & McFarlane, 1995), cloud microphysics (Gettelman et al., 2015), aerosol activation (Abdul-Razzak & Ghan, 2002) and shallow turbulence Golaz et al. (2002) are used in other models, so they feature similar or identical parameters. Beyond this, critical process treatments like auto-conversion and accretion (Khairoutdinov & Kogan, 2000), are described with similar parameters or using identical formulations in many models even with different parameterizations (Jing et al., 2019). It would be interesting to compare these results to those with other similar climate and weather models to ascertain if the behavior of individual processes is consistent, or if the process coupling within and between parameterizations induces different sensitivities. Some of the results are robust, like the importance of pre-industrial mean state suflate and CCN by Carslaw et al. (2013). This work could be repeated on mean state relationships using data that is part of the traditional Coupled Model Intercomparison (CMIP) archives, but the parameter-level analysis would require dedicated simulations.

Table A1. A description of the parameters that are perturbed and their ranges. Note for zmconv_ke units KE = (kg m^{-2} s^{-1})$^{0.5}$ s^{-1}

Physics Scheme	Parameter Name	Description	Default	Min	Max	Units
CLUBB	clubb_C2rt	Damping on scalar variances	1.0	0.2	2	-
	clubb_C6rt	Low skewness in C6rt skewness function	4.0	2.0	6	-
	clubb_C6rtb	High skewness in C6rt skewness function	6.0	2.0	8	-
	clubb_C6thl	Low skewness in C6thl skewness function	4.0	2.0	6	-
	clubb_C6thlb	High skewness in C6thl skewness function	6.0	2.0	8	-
	clubb_C8	Coef. #1 in C8 skewness Equation	4.2	1.0	5	-
	clubb_beta	Set plume widths for theta_l and rt	2.4	1.6	2.5	-
	clubb_c1	Low Skewness in C1 Skw.	1.0	0.4	3	-
	clubb_c11	Low Skewness in C11 Skw	0.7	0.2	0.8	-
	clubb_c14	Constant for u'^2 and v'^2 terms	2.2	0.4	3	-
	clubb_c_K10	Momentum coefficient of Kh_zm	0.5	0.2	1.2	-
	clubb_gamma_coef	Low Skw.: gamma coef. Skw	0.308	0.25	0.35	-
	clubb_wpxp_L_thresh	Lscale threshold, damp C6 and C7	60	20	200	m
MG2	micro_mg_accre_enhan_fact	Accretion enhancing factor	1.0	0.1	10.0	-
	micro_mg_autocon_fact	auto-conversion factor	0.01	0.005	0.2	-
	micro_mg_autocon_lwp_exp	KK2000 LWP exponent	2.47	2.10	3.30	-
	micro_mg_autocon_nd_exp	KK2000 auto-conversion exponent	-1.1	-0.8	-2	-
	micro_mg_berg_eff_factor	Bergeron efficiency factor	1.0	0.1	1.0	-
	micro_mg_dcs	auto-conversion size threshold ice-snow	500e-06	50e-06	1000e-06	m
	micro_mg_effi_factor	Scale effective radius for optics calculation	1.0	0.1	2.0	-
	micro_mg_homog_size	Homogeneous freezing ice particle size	25e-6	10e-6	200e-6	m
	micro_mg_iaccr_factor	Scaling ice/snow accretion	1.0	0.2	1.0	-
	micro_mg_max_nicons	Maximum allowed ice number concentration	100e6	1e5	10,000e6	# kg^{-1}
	micro_mg_vtrmi_factor	Ice fall speed scaling	1.0	0.2	5.0	m s^{-1}
Aerosol	microp_aero_npccn_scale	Scale activated liquid number	1	0.33	3	-
	microp_aero_wsub_min	Min subgrid velocity for liq activation	0.2	0	0.5	m s^{-1}
	microp_aero_wsub_scale	Subgrid velocity for liquid activation scaling	1	0.1	5	-
	microp_aero_wsubi_min	Min subgrid velocity for ice activation	0.001	0	0.2	m s^{-1}
	microp_aero_wsubi_scale	Subgrid velocity for ice activation scaling	1	0.1	5	-
	dust_emis_fact	Dust emission scaling factor	0.7	0.1	1.0	-
	seasalt_emis_scale	Seasalt emission scaling factor	1.0	0.5	2.5	-
	sol_factb_interstitial	Below cloud scavenging of interstitial modal aerosols	0.1	0.1	1	-
	sol_factic_interstitial	In-cloud scavenging of interstitial modal aerosols	0.4	0.1	1	-
ZM	cldfrc_dp1	Parameter for deep convection cloud fraction	0.1	0.05	0.25	-
	cldfrc_dp2	Parameter for deep convection cloud fraction	500	100	1,000	-
	zmconv_c0_lnd	Convective auto-conversion over land	0.0075	0.002	0.1	m^{-1}
	zmconv_c0_ocn	Convective auto-conversion over ocean	0.03	0.02	0.1	m^{-1}
	zmconv_capelmt	Triggering threshold for ZM convection	70	35	350	J kg^{-1}
	zmconv_dmpdz	Entrainment parameter	-1.0e-3	-2.0e-3	-2.0e-4	m^{-1}
	zmconv_ke	Convective evaporation efficiency	5.0e-6	1.0e-6	1.0e-5	KE
	zmconv_ke_lnd	Convective evaporation efficiency over land	1.0e-5	1.0e-6	1.0e-5	KE
	zmconv_momcd	Efficiency of pressure term in ZM downdraft CMT	0.7	0	1	-
	mconv_momcu	Efficiency of pressure term in ZM updraft CMT	0.7	0	1	-
	zmconv_num_cin	Allowed number of negative buoyancy crossings	1	1	5	-
	zmconv_tiedke_add	Convective parcel temperature perturbation	0.5	0	2	K

It is also clear that better constraining the warm rain process and ice processes in the atmosphere are critical for narrowing the uncertainty in climate forcing and feedbacks.

Appendix A Parameters

Table A1, based on Eidhammer et al. (2024), describes the parameters used in the PPE by physical parameterization, with formal name, description, default value, minimum, maximum and units.

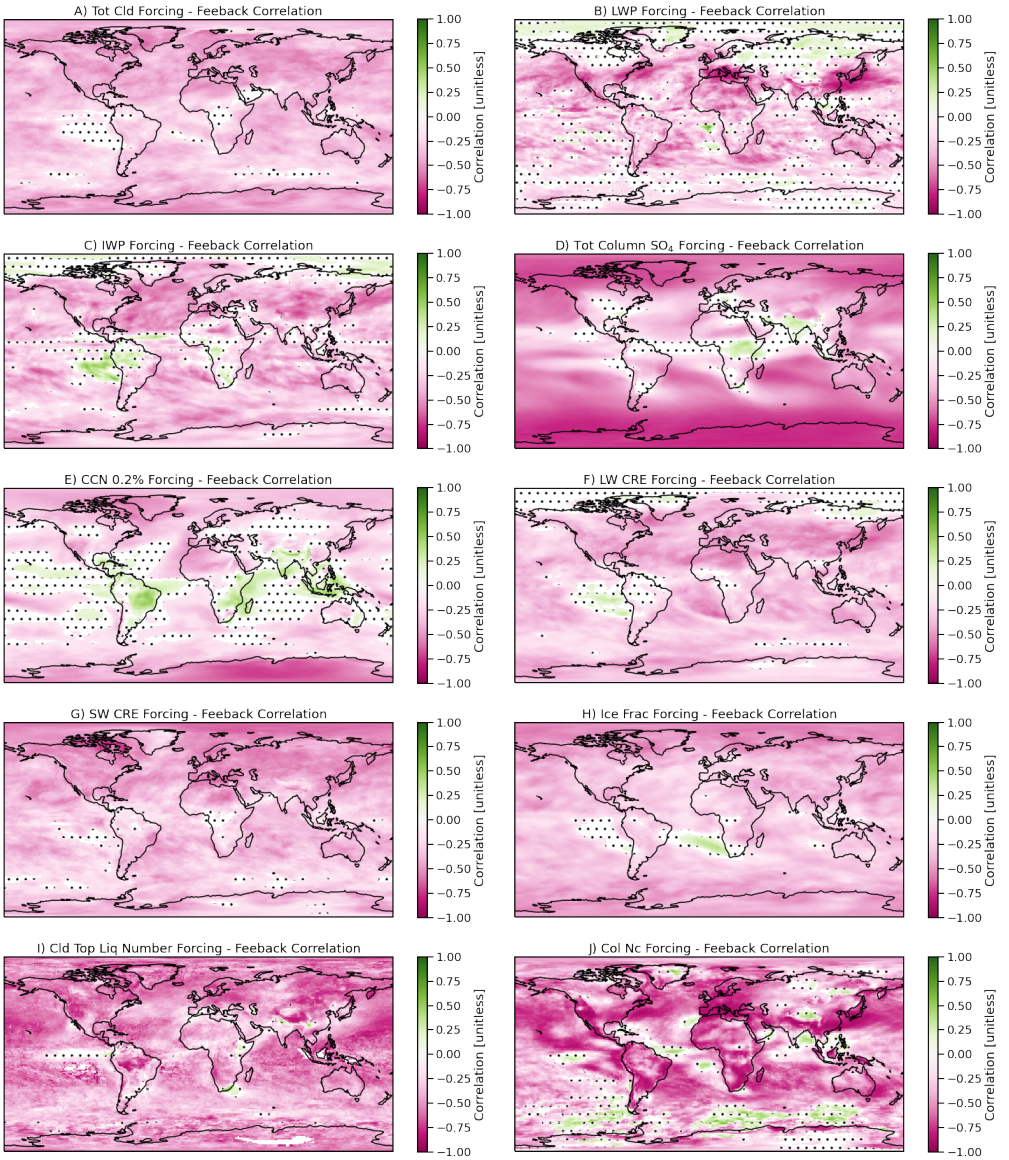

Figure B1. Map of linear correlation coefficient at each point between differences in variables due to forcing (PD-PI) and feedbacks (SST+4K - PD) for different variables. Non-significant points are stippled. Significance is determined by a bootstrap fit.

Appendix B Supplementary Figures

Appendix C Open Research

Model output used is described by Eidhammer et al. (2024), and is available the Climate Data Gateway at NCAR (https://doi.org/10.26024/bzne-yf09)

Analysis code used in this work is available on zenodo at https://zenodo.org/doi/10.5281/zenodo.10553073

Acknowledgments

NCAR is supported by the U. S. National Science Foundation. The Pacific Northwest National Laboratory is operated for the U.S. Department of Energy by the Battelle Memorial Institute under contract DE-AC05-76RL01830.

References

Abdul-Razzak, H., & Ghan, S. J. (2002). A parameterization of aerosol activation 3. Sectional Representation. *J. Geophys. Res*, *107*(D3), AAC 1-1 – AAC 1-6. doi: 10.1029/2001JD000483

Ackerman, A. S., Kirkpatrick, M. P., Stevens, D. E., & Toon, O. B. (2004). The impact of humidity above stratiform clouds on indirect aerosol climate forcing. *Nature*, *432*, 1014–1017.

Albrecht, B. A. (1989). Aerosols, Cloud Microphysics and Fractional Cloudiness. *Science*, *245*, 1227–1230. doi: 10.1126/science.245.4923.1227

Bellouin, N., Quaas, J., Gryspeerdt, E., Kinne, S., Stier, P., Watson-Parris, D., ... Stevens, B. (2020). Bounding Global Aerosol Radiative Forcing of Climate Change. *Reviews of Geophysics*, *58*(1), e2019RG000660. doi: 10.1029/2019RG000660

Carslaw, KS., Lee, LA., Reddington, CL., Pringle, KJ., Rap, A., Forster, PM., ... others (2013). Large contribution of natural aerosols to uncertainty in indirect forcing. *Nature*, *503*(7474), 67–71. doi: 10.1038/nature12674

Cess, R. D., et al. (1989). Interpretation of Cloud-Climate Feedback as Produced by 14 Atmospheric General Circulation Models. *Science*, *245*, 513–516.

Eidhammer, T., Gettelman, A., Thayer-Calder, K., Watson-Parris, D., Elsaesser, G., Morrison, H., ... McCoy, D. (2024, January). An Extensible Perturbed Parameter Ensemble (PPE) for the Community Atmosphere Model Version 6. *EGUsphere*, 1–27. doi: 10.5194/egusphere-2023-2165

Forster, P. M., Andrews, T., Good, P., Gregory, J. M., Jackson, L. S., & Zelinka, M. (2013, February). Evaluating adjusted forcing and model spread for historical and future scenarios in the CMIP5 generation of climate models: FORCING IN CMIP5 CLIMATE MODELS. *Journal of Geophysical Research: Atmospheres*, *118*(3), 1139–1150. doi: 10.1002/jgrd.50174

Gettelman, A., Gagne, D. J., Chen, C.-C., Christensen, M. W., Lebo, Z. J., Morrison, H., & Gantos, G. (2021). Machine Learning the Warm Rain Process. *Journal of Advances in Modeling Earth Systems*, *13*(2), e2020MS002268. doi: 10.1029/2020MS002268

Gettelman, A., Hannay, C., Bacmeister, J. T., Neale, R. B., Pendergrass, A. G., Danabasoglu, G., ... Mills, M. J. (2019). High Climate Sensitivity in the Community Earth System Model Version 2 (CESM2). *Geophysical Research Letters*, *46*(14), 8329–8337. doi: 10.1029/2019GL083978

Gettelman, A., Lin, L., Medeiros, B., & Olson, J. (2016, June). Climate Feedback Variance and the Interaction of Aerosol Forcing and Feedbacks. *J. Climate*, *29*(18), 6659–6675. doi: 10.1175/JCLI-D-16-0151.1

Gettelman, A., Morrison, H., Santos, S., Bogenschutz, P., & Caldwell, P. M. (2015). Advanced Two-Moment Bulk Microphysics for Global Models. Part II: Global Model Solutions and Aerosol–Cloud Interactions. *J. Climate*, *28*(3), 1288–1307. doi: 10.1175/JCLI-D-14-00103.1

Gettelman, A., & Sherwood, S. C. (2016, October). Processes Responsible for Cloud Feedback. *Curr Clim Change Rep*, 1–11. doi: 10.1007/s40641-016-0052-8

Golaz, J.-C., Larson, V. E., & Cotton, W. R. (2002). A PDF-Based Model for Boundary Layer Clouds. Part II: Model Results. *J. Atmos. Sci.*, *59*, 3552–3571.

Guo, H., Golaz, J.-C., Donner, L. J., Wyman, B., Zhao, M., & Ginoux, P. (2015, May). CLUBB as a unified cloud parameterization: Opportunities and challenges. *Geophys. Res. Lett.*, 2015GL063672. doi: 10.1002/2015GL063672

Guo, Z., Wang, M., Qian, Y., Larson, V. E., Ghan, S., Ovchinnikov, M., ... Zhou, T. (2015, July). Parametric behaviors of CLUBB in simulations of low clouds in the Community Atmosphere Model (CAM). *J. Adv. Model. Earth Syst.*, n/a-n/a. doi: 10.1002/2014MS000405

Jing, X., Suzuki, K., & Michibata, T. (2019, July). The Key Role of Warm Rain Parameterization in Determining the Aerosol Indirect Effect in a Global Climate Model. *Journal of Climate*, *32*(14), 4409–4430. doi: 10.1175/JCLI-D-18-0789.1

Khairoutdinov, M. F., & Kogan, Y. (2000). A new cloud physics parameterization in a large-eddy simulation model of marine stratocumulus. *Monthly Weather Review*, *128*, 229–243.

Kiehl, J. T. (2007, November). Twentieth century climate model response and climate sensitivity. *Geophys. Res. Lett.*, *34*(22), L22710. doi: 10.1029/2007GL031383

Lee, L. A., Reddington, C. L., & Carslaw, K. S. (2016, May). On the relationship between aerosol model uncertainty and radiative forcing uncertainty. *PNAS*, *113*(21), 5820–5827. doi: 10.1073/pnas.1507050113

Loeb, N. G., Doelling, D. R., Wang, H., Su, W., Nguyen, C., Corbett, J. G., ... Kato, S. (2018). Clouds and the Earth's Radiant Energy System (CERES) Energy Balanced and Filled (EBAF) Top-of-Atmosphere (TOA) Edition-4.0 Data Product. *J. Climate*, *31*(2), 895–918. doi: 10.1175/JCLI-D-17-0208.1

Qian, Y., Wan, H., Yang, B., Golaz, J.-C., Harrop, B., Hou, Z., ... Zhang, K. (2018). Parametric Sensitivity and Uncertainty Quantification in the Version 1 of E3SM Atmosphere Model Based on Short Perturbed Parameter Ensemble Simulations. *Journal of Geophysical Research: Atmospheres*, *123*(23), 13,046–13,073. doi: 10.1029/2018JD028927

Regayre, L. A., Deaconu, L., Grosvenor, D. P., Sexton, D. M. H., Symonds, C., Langton, T., ... Carslaw, K. S. (2023, August). Identifying climate model structural inconsistencies allows for tight constraint of aerosol radiative forcing. *Atmospheric Chemistry and Physics*, *23*(15), 8749–8768. doi: 10.5194/acp-23-8749-2023

Sherwood, S., Webb, M. J., Annan, J. D., Armour, K. C., Forster, P. M., Hargreaves, J. C., ... Zelinka, M. D. (2020). An assessment of Earth's climate sensitivity using multiple lines of evidence. *Reviews of Geophysics*, *58*(n/a), e2019RG000678. doi: 10.1029/2019RG000678

Sherwood, S. C., Bony, S., & Dufresne, J.-L. (2014, January). Spread in model climate sensitivity traced to atmospheric convective mixing. *Nature*, *505*(7481), 37–42. doi: 10.1038/nature12829

Smith, C. J., Kramer, R. J., Myhre, G., Alterskjær, K., Collins, W., Sima, A., ... Forster, P. M. (2020, January). Effective radiative forcing and adjustments in CMIP6 models. *Atmospheric Chemistry and Physics Discussions*, 1–37. doi: 10.5194/acp-2019-1212

Soden, B. J., Held, I. M., Colman, R., Shell, K. M., Kiehl, J. T., & Shields, C. A. (2008). Quantifying Climate Feedbacks Using Radiative Kernels. *J. Climate*,

21(14), 3504–3520. doi: 10.1175/2007JCLI2110.1

Summary for Policymakers. (2021). In Intergovernmental Panel on Climate Change (IPCC) (Ed.), *Climate Change 2021 – The Physical Science Basis: Working Group I Contribution to the Sixth Assessment Report of the Intergovernmental Panel on Climate Change* (pp. 3–32). Cambridge: Cambridge University Press. doi: 10.1017/9781009157896.001

Twomey, S. (1974). Pollution and the planetary albedo. *Atmospheric Environment (1967)*, *8*(12), 1251–1256.

Watson-Parris, D., & Smith, C. J. (2022, December). Large uncertainty in future warming due to aerosol forcing. *Nat. Clim. Chang.*, *12*(12), 1111–1113. doi: 10.1038/s41558-022-01516-0

Watson-Parris, D., Williams, A., Deaconu, L., & Stier, P. (2021, December). Model calibration using ESEm v1.1.0 – an open, scalable Earth system emulator. *Geoscientific Model Development*, *14*(12), 7659–7672. doi: 10.5194/gmd-14-7659-2021

Zelinka, M., Klein, S., & Hartmann, D. (2012). Computing and partitioning cloud feedbacks using cloud property histograms. Part I: Cloud radiative kernels. *J. Climate*, *25*(11), 3715–3735.

Zhang, G. J., & McFarlane, N. A. (1995). Sensitivity of climate simulations to the parameterization of cumulus convection in the Canadian Climate Center general circulation model. *Atmos. Ocean*, *33*, 407–446.

Zhang, H., Wang, M., Guo, Z., Zhou, C., Zhou, T., Qian, Y., ... Gettelman, A. (2018). Low-Cloud Feedback in CAM5-CLUBB: Physical Mechanisms and Parameter Sensitivity Analysis. *Journal of Advances in Modeling Earth Systems*, *10*(11), 2844–2864. doi: 10.1029/2018MS001423